The Thesis Committee for Christine Marie Egnatuk
Certifies that this is the approved version of the following thesis:

Identifying Short-Lived Fission Products by Delayed Gamma-Ray Emission

APPROVED BY
SUPERVISING COMMITTEE:

Supervisor:

Steven R. F. Biegalski

Sheldon Landsberger

Identifying Short-Lived Fission Products by Delayed Gamma-Ray Emission

by

Christine Marie Egnatuk, B.A.

Thesis

Presented to the Faculty of the Graduate School of

The University of Texas at Austin

in Partial Fulfillment

of the Requirements

for the Degree of

Master of Science in Engineering

The University of Texas at Austin

December 2009

Dedication

To Tracy and Jess.

Acknowledgements

I would like to thank Dr. Steven Biegalski for the guidance through this tumultuous process. I also would like to thank Dr. Landsberger for providing direction and prompt feedback. The data collection could not have been completed without the beam chopper built by Alex Brand and Larry Welch. I would also like to thank Mike Krause for providing the pictures of the reactor core.

I would like to acknowledge The Office of Naval Research and Quentin Saulter for providing the funding for this project.

December 4, 2009

Abstract

Identifying Short-Lived Fission Products by Delayed Gamma-Ray Emission

Christine Marie Egnatuk, M.S.E.
The University of Texas at Austin, 2009

Supervisor: Steven R. F. Biegalski

The prompt gamma-ray spectrum of uranium yields no substantial identifying peaks. Therefore, fission products created by a beam of thermal neutrons incident on the uranium sample must be examined in order to create a fingerprint to identify the sample. While neutron irradiation ceased, a high purity germanium detector was used to count photon emission by short-lived uranium fission products.

Two methods were used to examine the fission products. In each method uranium samples were irradiated for approximately 45 minutes to allow for the saturation of fission products. The first method used the beam port shutter and allowed for longer counting and irradiation times, but was unsuitable for examining fission products with half-lives below 10 seconds. The on/off method used a cycle of equal irradiation and

counting times of one minute. The second method is able to measure track the production of fission products with half-lives of less than 10 seconds. This method used a borated aluminum wheel beam chopper to stop the irradiation of the sample during counting. The beam chopper was set to cycle for approximately one second of counting following half a second of irradiation.

The spectra from both methods were analyzed and the peaks were assigned to the appropriate fission products. The majority of the peaks were composed of gamma-rays from multiple nuclides. The peaks created by gamma-rays from decays of a single nuclide were used to calculate the detection limits of the system. Using the beam chopper system, 21 peaks would be above the detection limits of our system 95% of the time for uranium samples of less than one kilogram.

Table of Contents

List of Tables

List of Figures

Chapter 1: Introduction

1.1 MOTIVATION

The duties, spending, and scope of The Department of Homeland Security have increased tremendously in this country since the first major terrorist attack on the mainland of the United States on September 11, 2001. In 2001 the spending on homeland security was 20.7 billion dollars. By 2006 the project budget for The Department of Homeland Security more than doubled to 49.7 billion dollars [1]. As the danger, or perceived threat, of terrorism continues The United States will consistently increase spending in the upcoming years to prevent any additional violence in this country due to terrorism.

The escalating tensions between the United States government and terrorist organizations has raised the concern that a future attack could include a nuclear component—a nuclear weapon or a dirty bomb, which could result in a radioactive contamination of a large area in addition to casualties. The threat of proliferation is always on the international stage because of loosened regulations for handling special nuclear materials in times and areas of governmental upheaval. A few decades ago, the major concern was the nuclear weapons stockpile of the former Soviet Union. However, the number of countries with nuclear capabilities has been increasing in the past decade.

Countries that have a hostile relationship with the United States have recently started developing nuclear programs. North Korea is believed to be close to developing a ballistic warhead to detonate a nuclear weapon. There are estimates that North Korea has enough plutonium to make six nuclear bombs [2]. According to Mohamed Elbaradei, the

past Director of the International Atomic Energy Agency (IAEA), Iran has a large amount of low enriched uranium, below 5% enriched. He claims Iran will be unable to enrich uranium to weapons grade [3] approximately 90% enriched uranium, while the IAEA inspectors are present in Iranian facilities. Uranium enrichment facilities, including hundreds of gas centrifuges, near Natanz in Iran have been discovered and consequently dismantled [4]. Whether or not Iran has the expertise to enrich uranium to weapons grade levels is unknown and currently being debated on the international stage.

The possibility of a large amount of special nuclear materials in the hands of aggressive countries puts the United States in a difficult position. The detection of nuclear materials is necessary for the monitoring and tracking of possible threats to the United States. It is also necessary to be able to distinguish between different types of nuclear materials, isotopes present and enrichment levels, with a variety of techniques. This allows our intelligence sector to have multiple methods to confirm or disprove a possible threat to the safety of the United States.

1.2 LITERATURE REVIEW

The detection of materials that are a security threat to the United States and other sovereign nations has been well researched. Groups around the world have taken different approaches to recognizing undesirable materials even when the materials are concealed. One group has developed a technique to examine the contents of suitcases to detect explosive devices [5]. Other groups have focused on the differentiation of different enrichment levels of uranium [6-8].

1.2.1 Using Delayed Neutrons

The presence or absence of uranium is frequently established by examining the delayed neutrons created from fission. After a sample is irradiated, the sample is counted using ^{3}He detectors [9]. The number of delayed neutrons counted is recorded. The mass of uranium in a sample has a linear correlation to the number of delayed thermal fission. This relationship has been extrapolated for calculating the ratio of ^{235}U to ^{238}U in a sample. Some methods require the separation of thorium from the sample, which yields a more accurate detection level. The percent ^{235}U by weight can be calculated using a fast neutron flux on the order of 10^{8} $n \cdot cm^{-2} \cdot s^{-1}$ with an error of only 0.02 w% in a sample with thorium removed [6]. In an attempt to calculate the amount of thorium in a sample and the ratio of ^{235}U to ^{238}U, the thorium was removed from the sample before the analysis of the uranium ratio. Unfortunately the thorium was destroyed in the removal process [7], so only an accurate measurement of the uranium ratio was calculated. One group established that the amount of uranium and thorium in the sample has a linear relationship with the delayed neutron counts divided by the weight of the sample. The slope of the line has evaluated to establish the uranium to thorium ratio within the sample. The larger slope results in a higher ratio of uranium to thorium [10].

Neutron activation analysis can also be used in conjunction with delayed-neutron counting to establish the amount of uranium and thorium in materials—aluminum-copper alloys and silicon samples. The gamma spectroscopy focused on the production of ^{239}Np—from the beta decay of ^{239}U produced from $^{238}U(n,\gamma)$—and ^{233}Pa—formed from the beta decay of ^{233}Th produced from $^{232}Th(n,\gamma)$. By incorporating the gamma spectroscopy, the samples were accurate on the order of parts per billion [11].

Examining the delayed neutrons produced from fission is also used to differentiate between ^{235}U and ^{239}Pu. However, the percent absolute yield of thermal fission from delayed-neutrons from ^{235}U is approximately twice the height of the absolute yields for ^{239}Pu. However the absolute yield of the thermal fission produced delayed neutrons of ^{235}U and ^{239}Pu exhibit a similar shape with respect to time [12,13]. Therefore, it is necessary to know the mass of the sample in order to differentiate a ^{235}U sample and a ^{239}Pu sample by this method.

When looking at materials or setting up safeguards, the mass of the material in question is rarely known. Delayed neutrons produced from fission are also used to identify special nuclear materials when the mass of the sample in question is unknown. The Differential Die-Away Analysis (DDAA) uses 14 MeV neutron pulses from neutron generators to penetrate cargo containers. The production of fast neutrons with a time behavior that is slower than the original neutrons is detected signifies the presence of special nuclear materials in the cargo [14]. Unfortunately this technique does not allow classification of the nuclides present or the enrichment of the material.

Another safeguards procedure for monitoring large areas is the delayed neutron activation analysis (DNAA). This method determines, using swipes, if fissile material is present in the area tested. The samples are irradiated in a high flux thermal reactor and then counted. This method only confirms that the presence or absence of fissile material. Unfortunately, this method has not been able to quantify the fissile material on the swipe and cannot distinguish between ^{235}U and ^{239}Pu. DNAA only requires a minimal amount of sample preparation and allows the analysis of a large number of samples in a short period of time [15].

1.2.2 Using Gamma-Ray Spectrometry

HPGe detectors are usually used for the differentiation of ^{239}Pu and ^{235}U samples if the mass of the sample is known [16]. However, HPGe detectors are expensive and delicate. Therefore, Swanberg et al. used plastic and liquid scintillators were used to classify a sample of known mass as ^{239}Pu or ^{235}U. Using an irradiation time of only 30 seconds, the gamma-rays were counted for 25 seconds and the counts were broken up into 10 2.5 second bins. The counts were normalized using the mass of the sample and each bin was examined. The shape of the decay curves for ^{235}U and ^{239}Pu was extremely similar. The plastic and liquid scintillators were only able to examine gamma-rays between 1.2 and 4 MeV. Unfortunately the data was able to determine the presence or absence of ^{235}U and ^{239}Pu, but the system was not accurate enough to differentiate between the two fissile materials [16].

1.2.3. Prompt Gamma-Rays

Verbinksi, Weber, and Sund [17] examined the prompt gamma-rays from >99.7% enriched thin foil samples of ^{235}U, ^{239}Pu, and ^{252}Cf. The ^{235}U and ^{239}Pu samples were examined during fission with thermal neutrons. The ^{252}Cf sample was examined during spontaneous fission. Using NaI detectors, the thin sources were counted. The gamma-ray energy fission for each sample was calculated, as well as the photons per MeV created from fission. The classification of the spectra from ^{235}U and ^{239}Pu would be even more difficult if there was addition noise—possibly from surround materials or background levels. The current method compares the total number of gamma-quanta per fission event of ^{239}Pu and ^{235}U spectra, which is computationally extensive. Unfortunately, the differences between ^{239}Pu and ^{235}U are subtle for photons with energy

below 0.7 MeV and almost indistinguishable for photon energies from 0.7 MeV and 8 MeV [17].

Peelle and Maienschein [18] examined a sample of ^{235}U during thermal neutron fission. The photons between 0.01 MeV and 10 MeV were measured using a pair of NaI detectors. The data agrees with the findings of Verbinski, Weber, and Sund [17] on the values of gamma-ray energy per fission and photons per MeV of fission. However, the prompt spectra collected for both the ^{235}U and ^{239}Pu samples are extremely similar. The spectra require a thorough comparison to differentiate the samples. The prompt gamma-ray spectrum of ^{239}Pu has only a few major peaks, as shown in Figure 1.1, but the peaks are not large enough to allow for differentiation from other nuclides.

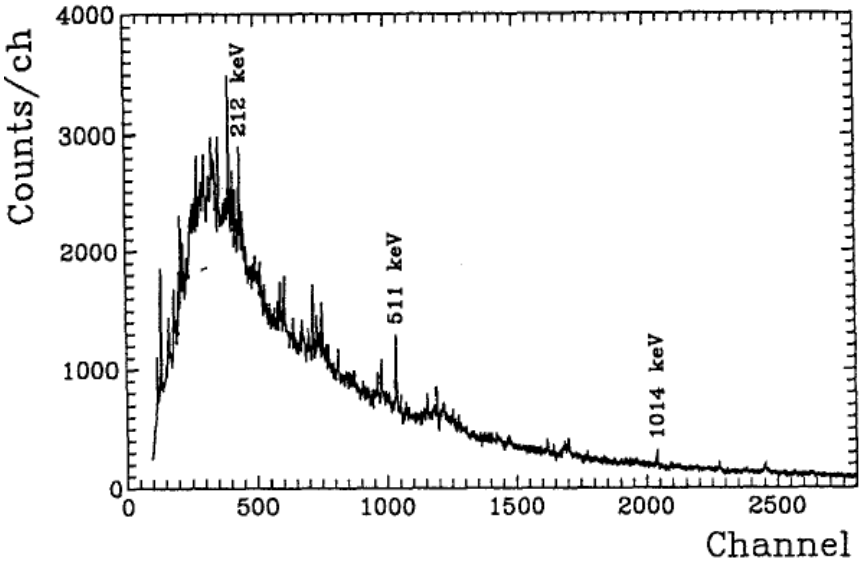

Figure 1.1: The $^{239}Pu(n,f)$ spectrum [19].

One of the main obstacles to detection is subtracting out the surrounding material to uncover the substance of interest. There are several groups using prompt gamma activation analysis to collect spectra through different mediums. This technique raises difficulties including the shielding and attenuation properties of the material. Recently there has been gamma-ray spectra collection using 14 MeV neutron generators [10, 14, 20, 21]. High energy neutrons are able to travel farther through materials, which makes shielding materials more difficult. Also, 14 MeV deuterium-tritium neutron generators are common and transportable [5, 20]. In order to create more portable methods of detection, NaI(T1) detectors and BaF_2 scintillators have been used to determine the material composition within different mediums [21].

Sixty-four neutron beams produced by a deuterium-tritium sealed neutron generator were used to examine the alpha-gamma coincidence time spectra of different samples while the sample is submerged in water [20]. The acquisition times are currently on the order of hours. However, the signatures of C, N, O, Na, Al, Si, Cl, K, Ca, Cr, Fe, Ni, Cu, Zn, and Pb have been established using the experimental data. The data collected experimentally has been compared with Monte Carlo calculations, but the computational calculations and experimental data do not agree below for the detection of particles below 14 MeV.

A similar approach was used to examine graphite, water, and melamin buried under ground. In this study, a NaI(T1) scintillator was used in conjunction with a BaF_2 scintilator [21]. The time difference between the detection of the gamma-ray and the alpha particle was used to calculate the travel distance of the fast neutrons emitted from the 14 MeV deuterium-tritium neutron generator. The BaF_2 scintilator provided the

timing necessary for the time difference calculation, but yielded sub-par resolution. The group ran into problems with oxygen detection due to the high oxygen content in the soil due to the soil moisture levels. Ultimately, the group was unable to differentiate between the materials and the blank sample while the materials were buried.

1.2.4 Fission Products

The fission products created in thermal fission of ^{239}Pu and ^{235}U were examined using Compton-suppressed germanium detectors and two x-ray detectors operating in coincidence [22]. The group examined the products created 10^{-21} to 10^{-12} seconds after the induced fission, which is referred to as the prompt time period. The spectra created from the fission products for both ^{239}Pu and ^{235}U, shown in Figure 1.2 and Figure 1.3, show a large number of identifiable peaks that are attributed to the decay of different fission products.

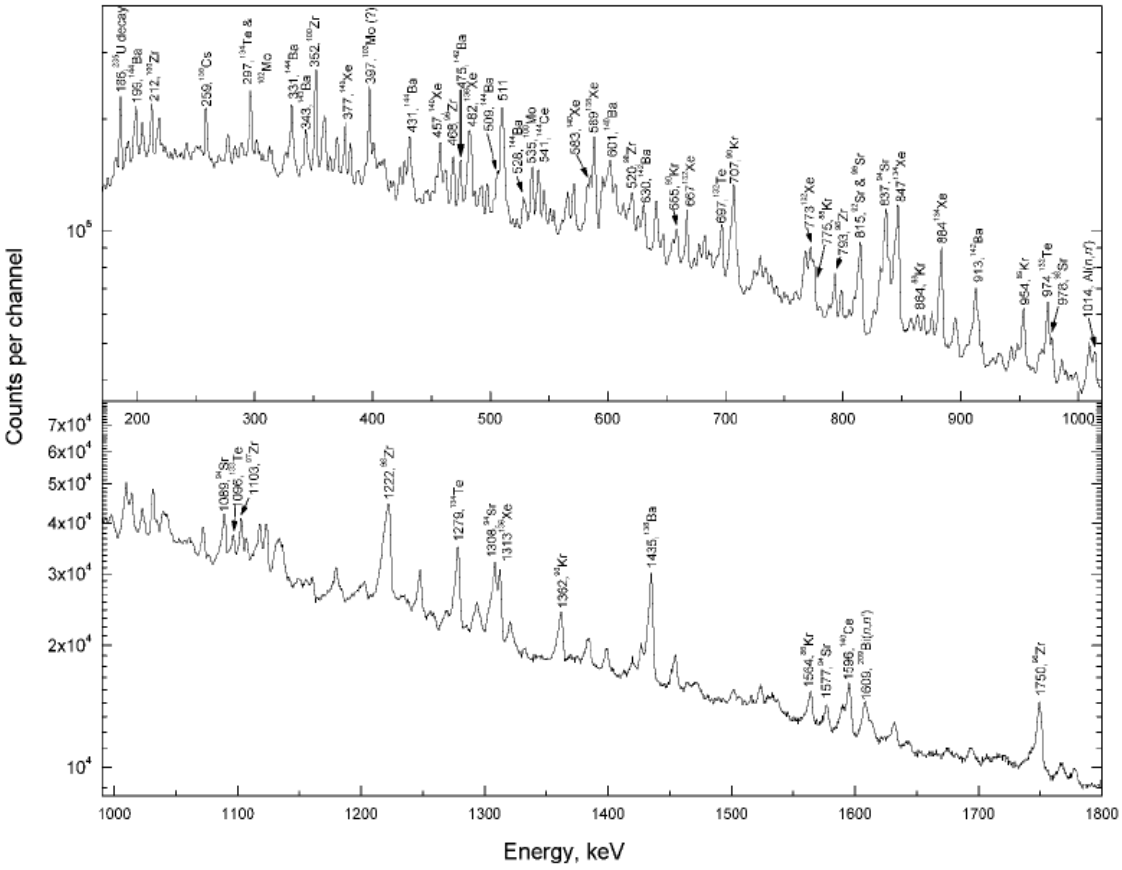

Figure 1.2: The ^{235}U(n,f) coincident gamma-ray spectrum [22].

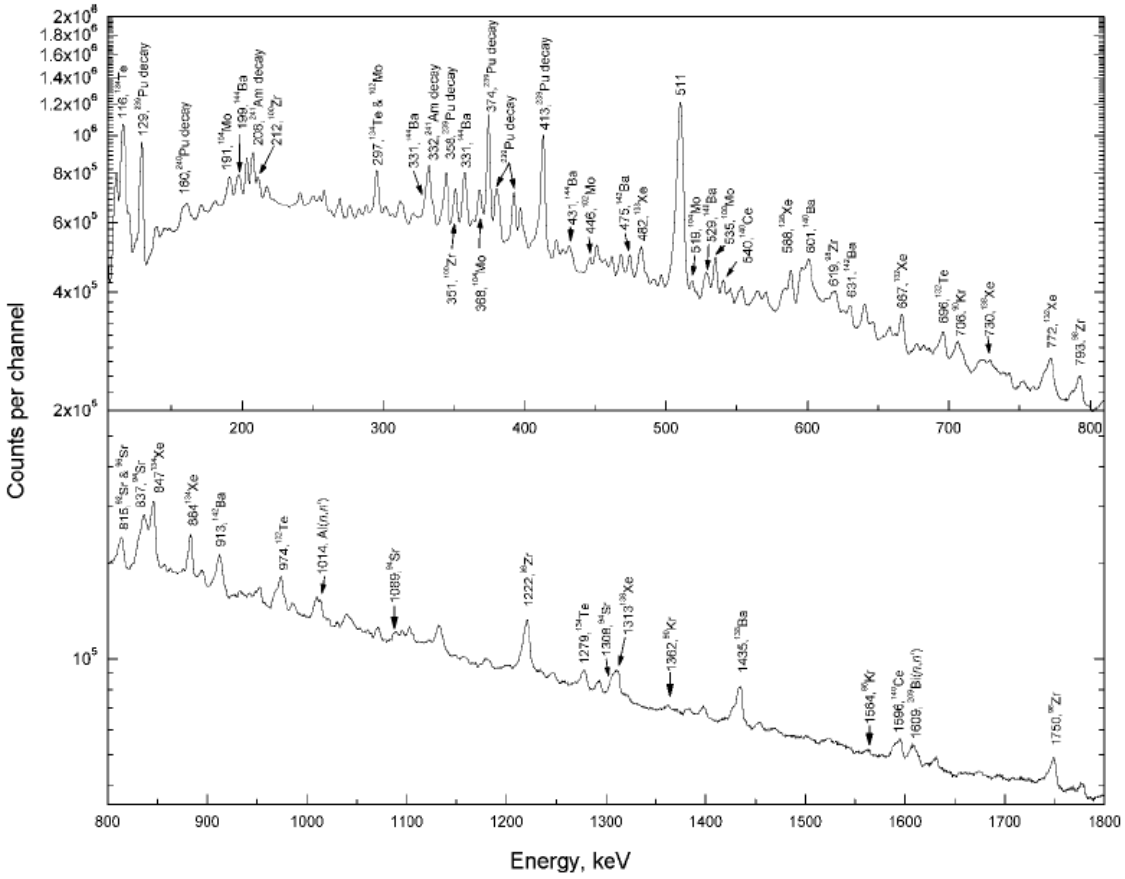

Figure 1.3: The ^{239}Pu(n,f) coincident gamma-ray spectrum [22].

Fissions that result in three fragments are relatively rare. Specifically, the focus was placed on examining the two fission fragments, the zero to six neutrons created, and the seven to ten prompt-gamma-rays released during the prompt time period [22]. Fission product pairs were selected for uranium—^{134}Te/Zr, ^{138}Xe/Sr, and ^{144}Ba/Kr—and plutonium—^{134}Te/Mo, ^{138}Xe/Zr, and ^{142}Ba/Sr. The number of neutrons of the denominator isotope is another variable used to differentiate between fission isotopes

with different mass numbers. The most conclusive way to differentiate between the isotopes of uranium and plutonium compares the ratios of these fission product pairs.

1.2.5 Delayed Gamma-Rays

A beam chopper at the Budapest Research Reactor allows the counting of the prompt gammas of a sample while simultaneously collecting the delayed spectrum [8]. Some of the decay lines of short-lived reactions appear in the prompt spectra, like the 1779 keV line of ^{28}Al. Since the detection limits are lower during the delayed counting time, more decay lines are present and not overwhelmed by the peaks from prompt gamma-rays [23]. The enrichment of two uranium samples was calculated by comparing an in-beam, or prompt spectrum, to a decay spectrum, shown in Figure 1.4. The spectra were collected used a beam chopper set to 25 Hz. The in-beam data was collected during the 20 ms irradiation time. This was followed by a 16ms decay phase when the decay data was collected [8].

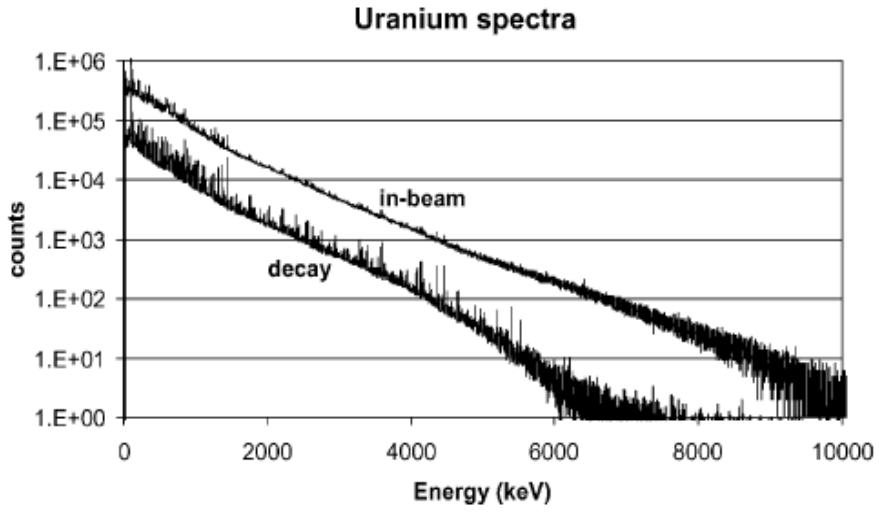

Figure 1.4: Uranium spectra acquired using the beam chopper at 25 Hz [8].

From the prompt spectrum, the ratio of the 6395 keV peak from the ^{235}U and the 4060 keV peak from the ^{238}U was examined. This ratio was then used to determine the ratio of ^{235}U to ^{238}U. The decay spectrum was used to subtract out the interference at the 4060 keV peak from the short-lived fission product ^{90}Rb. This allowed the group to differentiate between two uranium samples. On sample was enriched to 19.1% and the second sample was enriched to 36% [8].

1.3 GOALS

Using prompt gamma activation analysis alone, the prompt spectra of uranium and plutonium are difficult to differentiate quantitatively [17]. Therefore, the delayed gamma-rays of the fission products are examined in order to overcome this problem.

Using a cycle of irradiating the sample and pausing the irradiation while counting, the spectrum provides information about the fission products present in the sample.

Since the sample being irradiated contains ^{238}U, the timing must be considered to avoid ^{239}U photopeaks overwhelming the spectrum. The half-life of ^{239}U is 23.45 minutes. Therefore, the experiments used an irradiation and counting cycle time of one minute or less. The on/off method was used for one minute irradiation and counting times. A beam chopper was constructed to examine fission products with half-lives of less than 5 seconds.

The delayed gamma-rays allowed the identification of the short lived fission products present in the sample. However, there are multiple problems encountered while trying to classify the photopeaks in the fission product spectra. Lower energy gamma-rays are easily overwhelmed by gamma-rays from long-lived decay products [22]. While high energy gamma-rays are less affected by shielding and attenuation, the detector efficiency is lower at higher energy levels. The detection limits for the peaks at different energy levels created by a single nuclide show the amount of ^{235}U necessary for detection. This provides a solid number to compare across the energy levels and for different fission products.

Chapter 2: Theory

2.1 RADIATION

The decay of a radionuclide occurs when an unstable nucleus spontaneously emits ionizing particles and radiation. One form of radioactive decay releases an alpha particle, which is a charged ^{4}He nucleus. This type of decay happens in nuclei that are lacking neutrons. An example is the decay of ^{238}U that results in the production of ^{234}Th and an alpha particle

$$^{238}_{92}U \rightarrow ^{234}_{90}Th + ^{4}_{2}He \tag{2.1}$$

Another type of radioactive decay is beta decay. A positron, or beta-ray, and a neutrino are emitted during β^+ decay. For example,

$$^{15}O \xrightarrow{\beta+} ^{15}N + \upsilon \tag{2.2}$$

For nuclei that have too many neutrons, β^- decay occurs. This form of decay emits an electron and an anti-neutrino. For example,

$$^{19}O \xrightarrow{\beta-} ^{19}F + \bar{\upsilon} \tag{2.3}$$

The frequency of decay of any given nuclide can be described by its half-life. The half-life, $T_{\frac{1}{2}}$, of a nuclide is the amount of time it takes for a sample to decrease to one-half of its original quantity. The decay constant is frequently used instead of the half-life. The decay constant, λ, is defined as

$$\lambda = \frac{\ln 2}{T_{\frac{1}{2}}} \tag{2.4}$$

The activity of a sample is the number of disintegrations per unit time. The activity at time t can be described by the decay constant as

$$A(t) = A_0 e^{-\lambda t} \tag{2.5}$$

where A_0 is the initial activity of the sample.

2.2 FISSION

Fission occurs when a neutron interacts with a certain type of nuclei. The colliding neutron causes the nucleus to split apart and creates two or more fission products, some amount of neutrons, and the release of energy. A material that is capable of undergoing fission is referred to as a fissile material. As fission occurs, neutrons released from atomic splitting continue on and interact with other fissile material created what is referred to as a chain reaction.

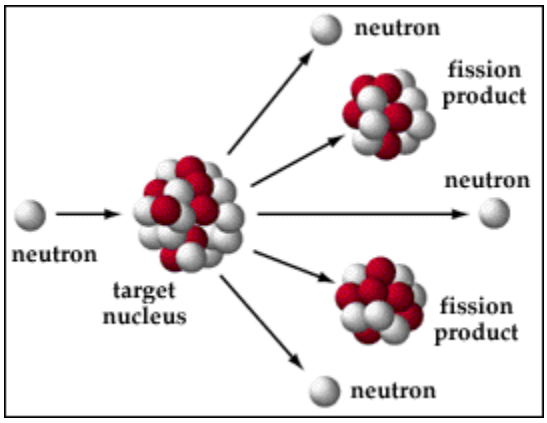

Figure 2.1: The target nucleus is hit by a neutron and produces several fission products and neutrons [24].

Fissile material is necessary for fission, but fertile material can help with the propagation of the reaction. A fertile substance is a material that can be converted into

fissionable, or fissile, material. For example, ^{238}U can be converted into ^{239}Pu, which is a fissionable material.

A single neutron induced fission, referred to as generation 1 in Illustration 2.2 can cause the production of multiple neutrons. The neutrons, referred to as generation 2 in Illustration 2.2, are able to collide with additional nuclei to induce fission. The increasing number of neutrons in the system increases the number of fissions. This phenomenon is referred to as a nuclear chain reaction.

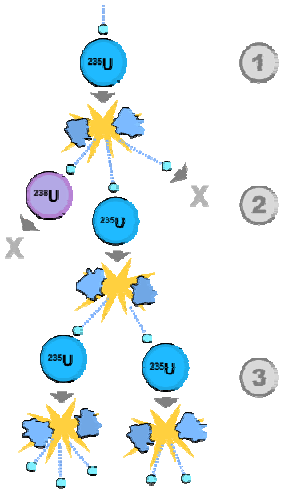

Figure 2.2: Chain reaction induced by a neutron fission event [25].

2.3 Fission Products

There are usually two different fission products created from fission, and the nucleus is rarely divided equally. This results in fission fragments that are dissimilar in mass number. In order create a more symmetric division of the nuclei during fission, the energy of the colliding neutron can be increased, as shown in Figure 2.3.

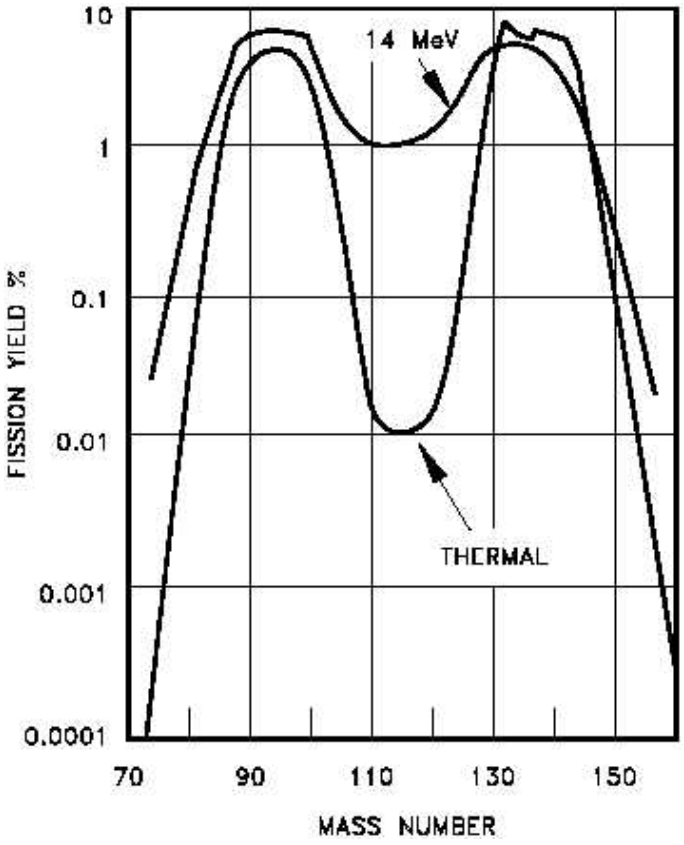

Figure 2.3: Fission product yields for thermal and 14-MeV fission neutrons in ^{235}U [26].

The fission products usually have too many neutrons to be stable. Therefore, the fission products undergo a sequence of β-decays, which results in a stable nuclide. In this case, ^{115}Pd undergoes several decays to produce ^{115}In, a stable nuclide.

$$^{115}Pd \xrightarrow{\beta-} {}^{115}Ag \xrightarrow{\beta-} {}^{115}Cd \xrightarrow{\beta-} {}^{115}In \qquad (2.6)$$

In order to calculate the amounts of certain fission products in a sample, the amount created by a nuclide produced by fission must be supplemented with the amount of the nuclide produced in decay chains.

During radioactive decay gamma-rays are frequently emitted. The frequency of emission is dependent on the nuclide undergoing the transformation and the initial energy level of the parent nuclide. The frequency of a nuclide emitting a gamma-ray, or the gamma-ray yield, at a given energy during radioactive decay is shown in the decay scheme, as shown in Figure 2.4.

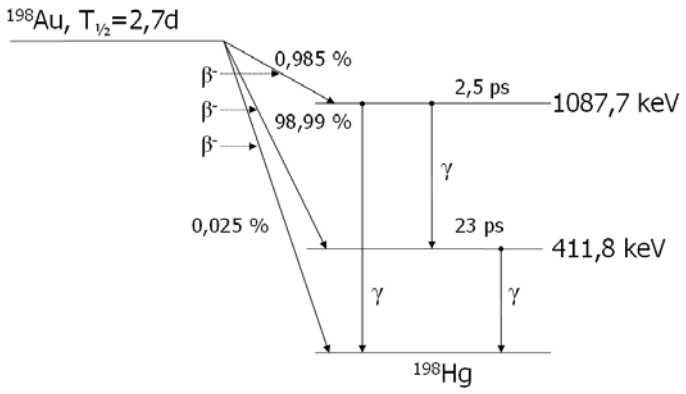

Figure 2.4: The decay scheme of ^{198}Au [27]

When using a detector system to count the gamma-rays at specific energy levels, the number of counts for a specific channel can be calculated by

$$\frac{counts}{channel} = A \cdot t \cdot \varepsilon \cdot \gamma_i \qquad (2.7)$$

where A is the activity of the sample in Becquerel, t is the time the sample is counted in seconds, ε is the efficiency of the detector for the channel, and γ_i is the gamma-ray yield for the specific energy.

2.4 PROMPT GAMMA ACTIVATION ANALYSIS

Prompt Gamma Activation Analysis is a nondestructive analytical technique used to quantitatively determine the different nuclides within a sample. In this process, a beam of neutrons is used to irradiate a sample of unknown composition. Interaction between the nuclei of the sample atoms and the incident neutrons allows for neutron capture and subsequent excitation to a higher but unstable energy state. For example, nitrogen and a neutron combine into an unstable nuclide, ^{15}N

$$^{14}N + n \rightarrow ^{15}N \tag{2.8}$$

The radioactive state the sample atoms are ephemeral, quickly decaying to a lower energy state and emitting gamma-ray photons of a specific energy. The gamma-ray released is dependent upon the nuclei of interaction. To continue the example, the ^{15}N releases a prompt gamma-ray, γ, and settles into a stable state.

$$^{15}\text{N} \rightarrow ^{15}\text{N} + \gamma \tag{2.9}$$

The emitted γ radiation is collected by a solid state, semiconductor, photon detector and binned based on their energy. Data acquisition software is then used to deconstruct the signal and develop of spectrum based on the gamma-ray energies, effectively fingerprinting the atomic composition of the sample. Due to the characteristic energies of emitted gamma-ray photons from specific elements, this spectrum can be used to determine the elemental composition of the supplied sample. The prompt gamma-ray spectrum for nitrogen is shown in Figure 2.5. Each photopeak denotes a gamma-ray of a certain energy released. The size of the peak is dependent on the activity of the sample, the absolute yield of the gamma-ray at that energy, and the detector efficiency at that energy.

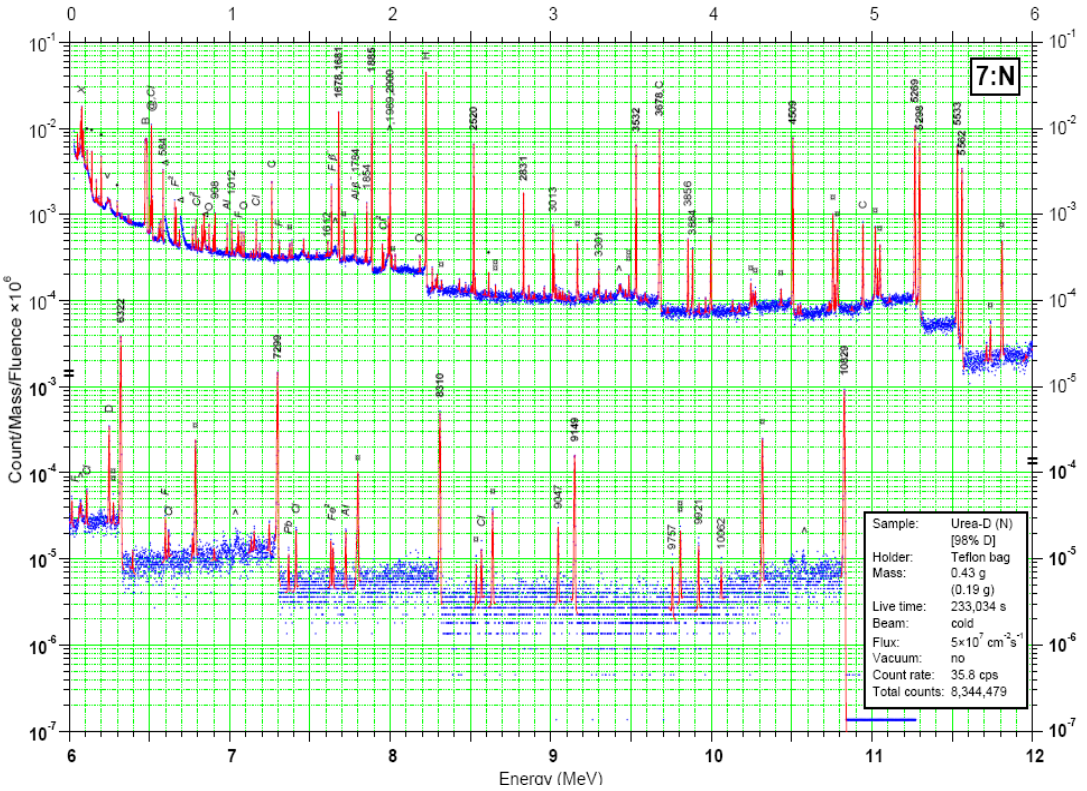

Figure 2.5: The prompt gamma spectrum for nitrogen [28].

2.5 PROMPT GAMMA-RAY ACTIVATION ANALYSIS OF SPECIAL NUCLEAR MATERIALS

The prompt gamma-ray spectrum produced by thermal neutron induced fission of natural uranium is shown in Figure 2.6. The ^{239}Pu prompt gamma-ray spectrum is shown in Figure 2.7. The uranium spectrum has a few large peaks attributed to the irradiation of ^{238}U. The ^{239}Pu spectrum only has small peaks that are not easy to distinguish from the background.

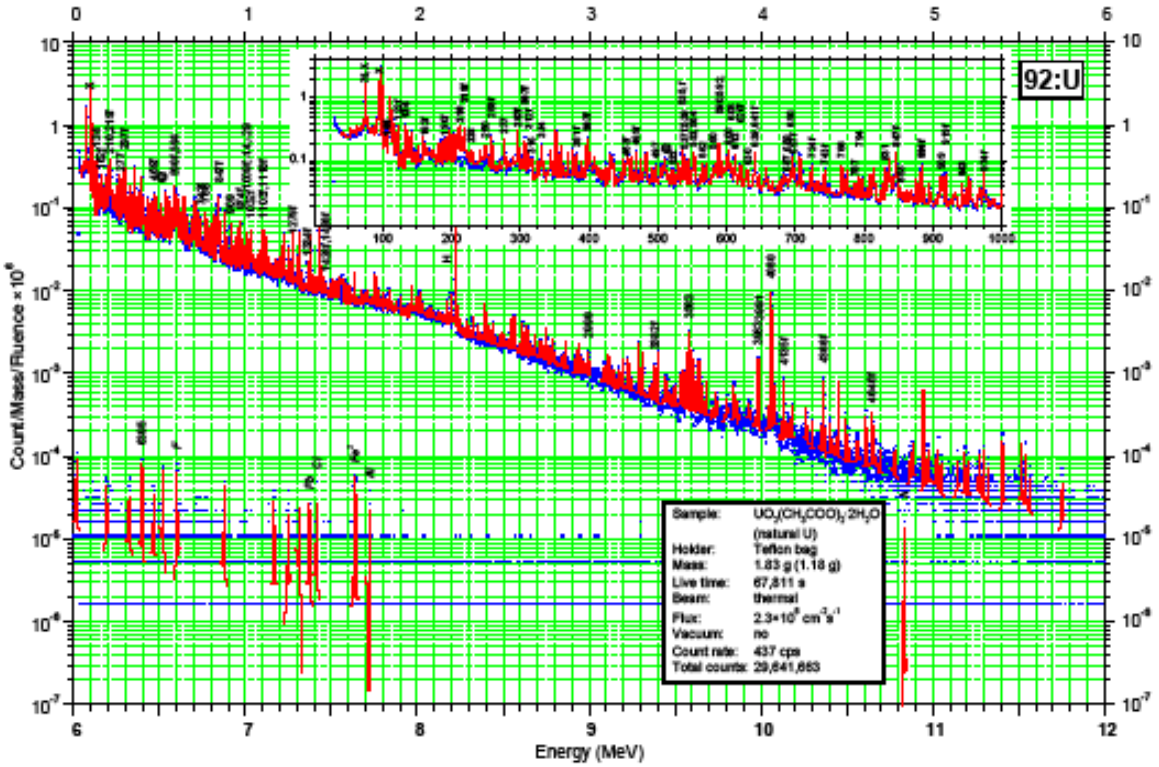

Figure 2.6: Uranium prompt spectrum [28].

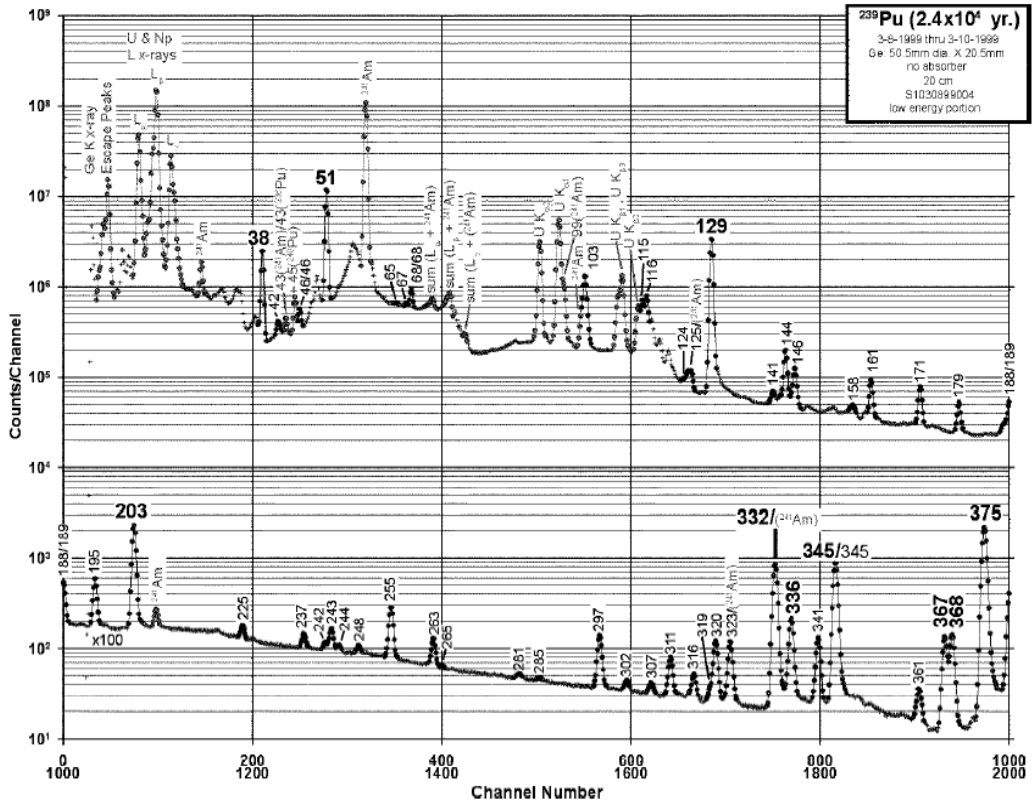

Figure 2.7: The prompt spectrum of ^{239}Pu [29].

The energy spectrum from the prompt photons from fission of ^{235}U is similar to energy spectra produced by other fissioning isotopes. Therefore, the ^{235}U spectrum is frequently used to approximate other isotopes. The data collected by Verbinski, Weber and Sund, shown in Figure 2.8, shows the close relationship in energy of prompt gamma-rays produced during thermal neutron induced fission for ^{239}Pu and ^{235}U [17].

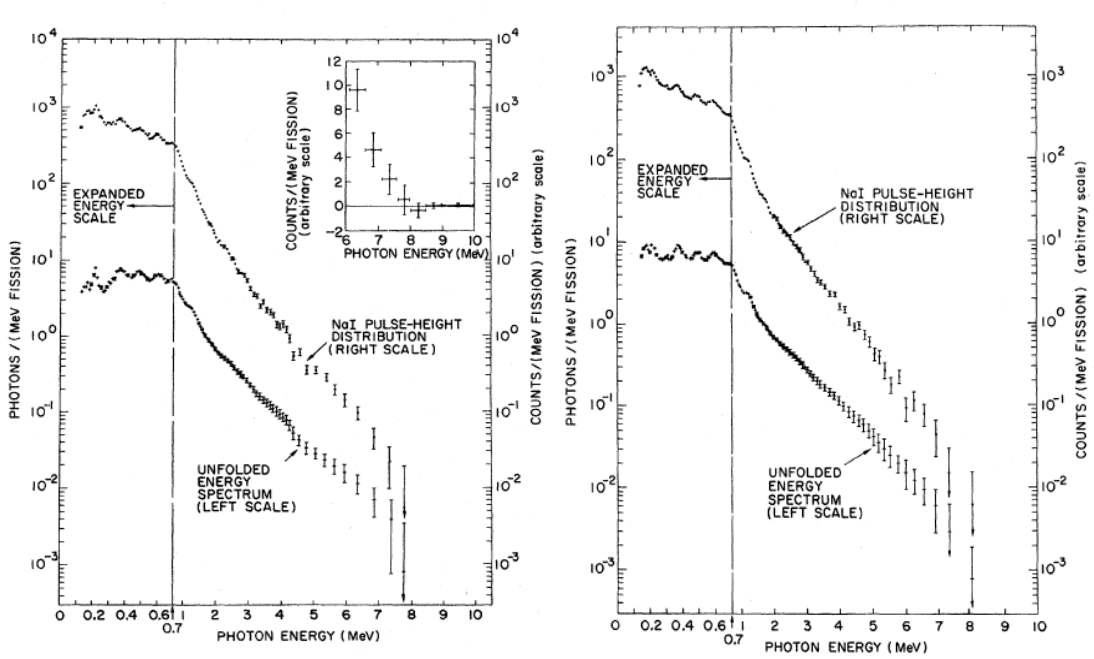

Figure 2.8: The prompt gamma-ray energy compared to the energy per fission from the thermal-neutron fission of ^{235}U is shown on the left. The right graph shows the prompt gamma-rays from the thermal-neutron fission of ^{239}Pu [17].

Using the photons emitted in coincidence with the thermal neutrons emitted during fission, the following empirical relationship was developed [18]

$$N_{p\gamma}(E) = \begin{cases} 6.6 & 0.1 < E < 0.6 MeV \\ 20.2e^{-1.78E} & 0.6 < E < 1.5 MeV \\ 7.2e^{-1.09E} & 1.5 < E < 10.5 MeV \end{cases} \qquad (2.10)$$

where $N_{p\gamma}(E)$ is the number of photons per MeV per fission and E is the energy of the photon in MeV. Equation (2.10) also closely resembles the empirical relationship of the exponential superposition described by Keepin [30] for the photons in the energy range of 0.3 MeV < E_γ < 7 MeV.

$$\frac{dN(E_\gamma)}{dE_\gamma} = 6.7e^{-1.05E_\gamma} + 30e^{-3.8E_\gamma} MeV^{-1} \qquad (2.11)$$

The empirical relationships described in equations (2.10) and (2.11) are compared to the data collected by Verbinski, Weber, and Sund in Figure 2.8. The empirical formulas provide a relatively close fit, as shown in Figure 2.9, to both the uranium and plutonium data collected experimentally by Verbinski, Weber, and Sund [17].

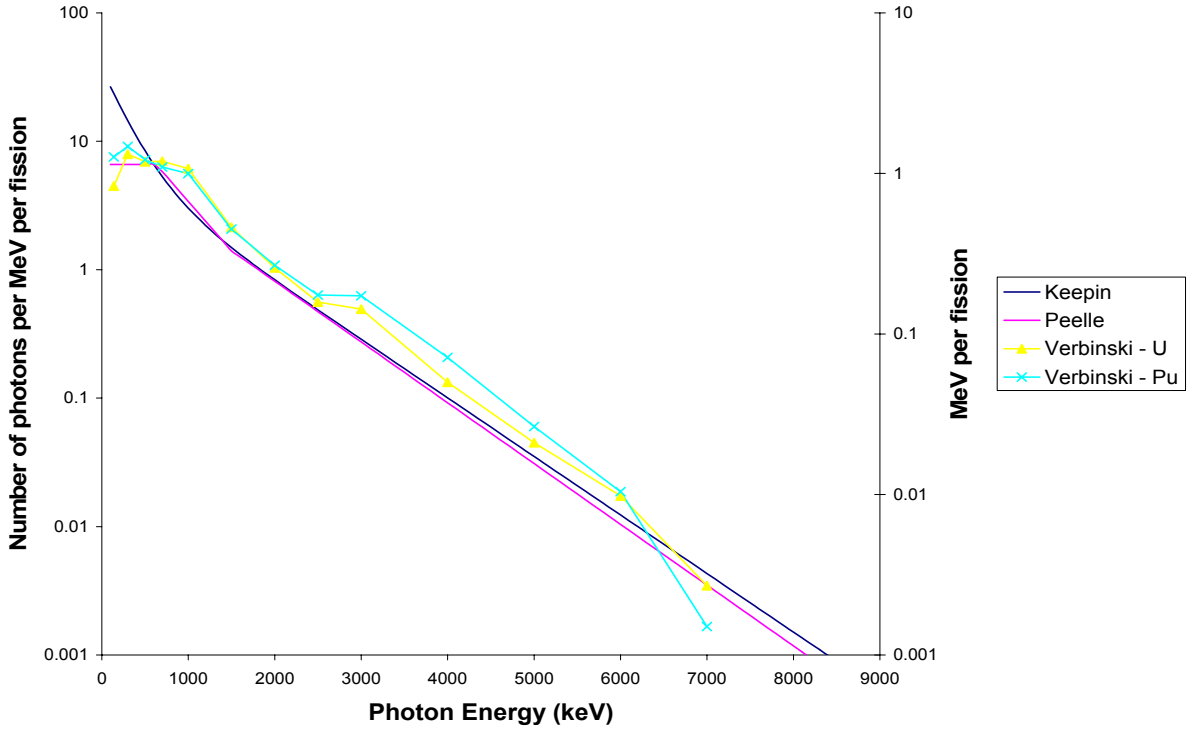

Figure 2.9: The empirical formulas [18, 30] compared to both the uranium and plutonium data collected by Verbinski, Weber, and Sund [17].

2.6 DETECTION LIMITS

The limiting levels for detection are defined by L_C, L_D, and L_Q. L_C is the net signal level that a signal may be detected if the signal is above. This critical level can be defined as

$$L_C = k_\alpha \sigma_0 \tag{2.12}$$

where k_α is the abscissas of a standardized normal distribution corresponding to a probability of 1-α, α is the probability of a false positive, and σ_0 is the standard deviation of a net signal when the limiting mean of the net signal is equal to zero.

The detection limit, L_D, is the net signal level that leads to detection. This can be described in terms of L_C as

$$L_D = L_C + k_\beta \sigma_D \tag{2.13}$$

where k_β is the abscissas of a standardized normal distribution corresponding to a probability of 1-β, β is the probability of a false negative, and σ_D is the standard deviation when the limiting mean of the net signal is equal to L_D.

The relationship between L_C, L_D, L_Q and other variations of error analysis is shown in Figure 2.10. The limiting levels consider detection sensitivity, sensitivity, minimum detectable activity, and limit of guarantee for purity.

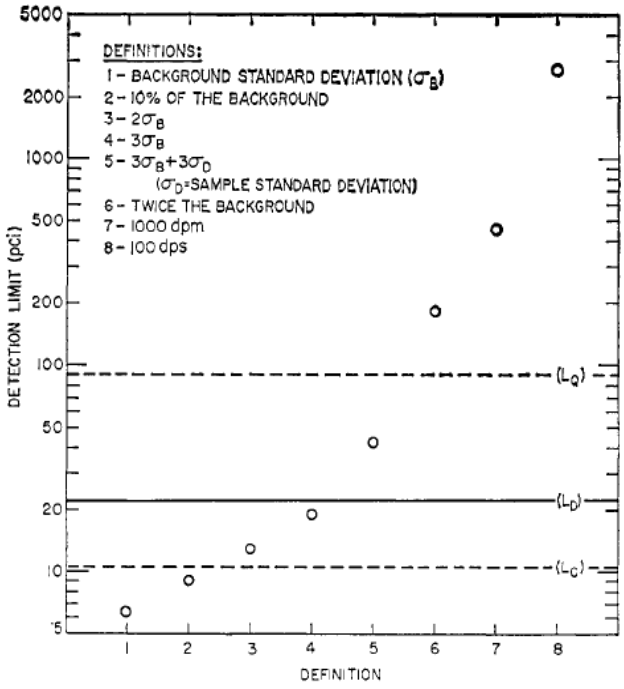

Figure 2.10: The L_C, L_D, and L_Q compared to alternative definitions for detection limits [31].

If the number of counts is sufficiently large and we can assume a normal distribution, the variance of the number of counts is

$$\sigma^2 = \sigma_{S+B}^2 + \sigma_{\bar{B}}^2 = (\mu_S + \mu_B) + \frac{\mu_B}{n} \qquad (2.14)$$

where σ_{S+B}^2 is the variance of the gross signal, $\sigma_{\bar{B}}^2$ is the variance of the blank, μ_S is the limiting mean of the net signal, and μ_B is the limiting mean of the blank. Allowing $k_\alpha=k_\beta$, the relationship for the detection limit in counts can be described by

$$L_D = k^2 + 2k\sqrt{2\mu_B} \qquad (2.15)$$

where $k= k_\alpha=k_\beta$ [31].

Chapter 3: Experimental Set-Up

3.1 THE REACTOR FACILITY

The reactor facility at the University of Texas at Austin is located in the Nuclear Engineering Teaching Laboratory on the Pickle Research Campus. The facility houses the 1.0 MW Mark II TRIGA (Training, Research, Isotopes, General Atomics) reactor used to conduct the experiments detailed in this study.

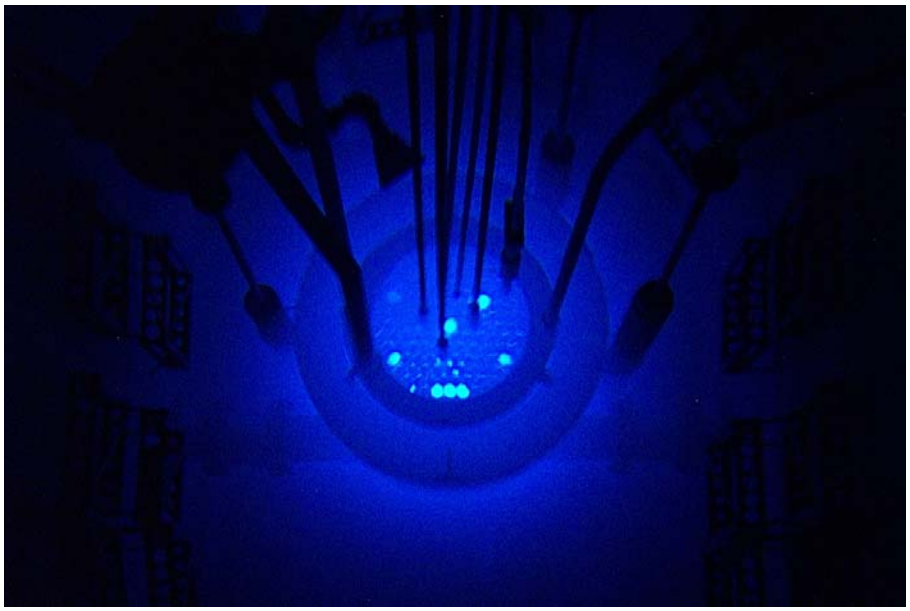

Figure 3.1: The core of the TRIGA reactor at The University of Texas.

The TRIGA Mark II reactor has a fixed center with four B_4C control rods and a reactor core composed of a fuel assembly that includes 104 fuel rods. Reactor power is generated by uranium zirconium hydride fuel enriched to 19.7 percent. The core is cooled by a water pool that immediately surrounds the reactor core and serves to attenuate

neutron kinetic energy. The core is surrounded by a graphite reflector scatters neutrons back into the system for another chance for fission.

Fission inside the reactor is initialized with an AmBe neutron source. The americium is surrounded by beryllium. An americium core produces alpha particles which interact with a beryllium shell surrounding the americium to produce neutrons. These neutrons are used to increase the number of neutrons in the reactor core during reactor start-up.

3.2 BEAM PORT THREE

3.2.1 Set-up

The beam port that houses the prompt gamma set-up used in this experiment is a radial beam port utilizing neutrons from the Mark II TRIGA reactor. The beam port set-up is shown in Figure 3.2.

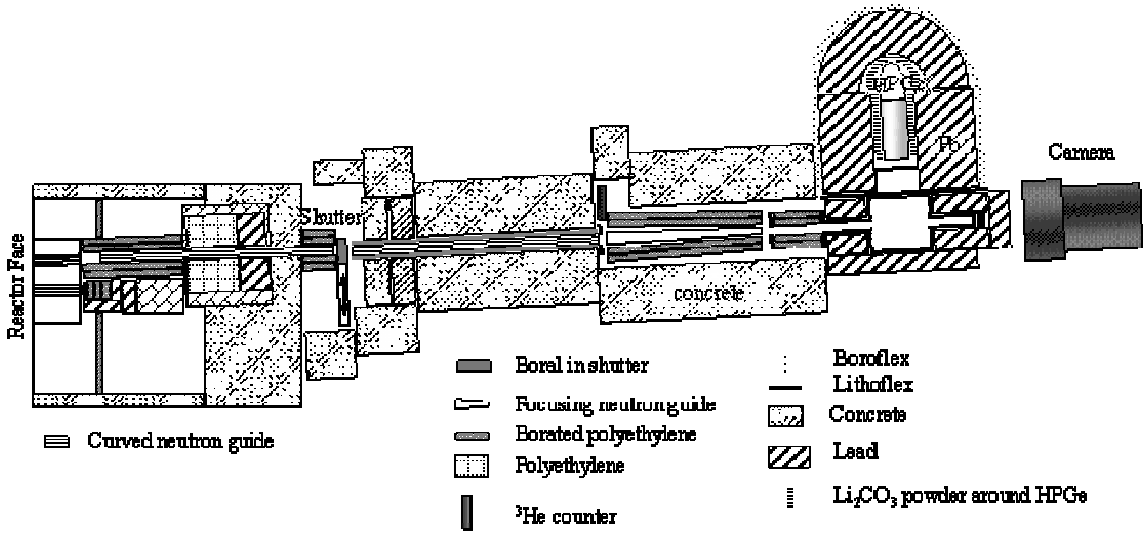

Figure 3.2: The set-up and shielding of beam port three at the University of Texas reactor facility[32].

Neutrons generated within the reactor core are funneled down a curved beam guide to separate out any neutrons that are not in the thermal range necessary for PGAA. This beam guide is encased in concrete and lead for safety purposes; it can be seen in Illustration 3.2. The flux of the neutron beam is $4x10^{6}$ $n \cdot cm^{-2} \cdot s^{-1}$ [33]. The sample to be examined is placed in front of the collimated beam of neutrons at the end of beam port three. Atoms within the sample absorb some of the incident neutrons and upon subsequent energy relaxation, emit gamma-ray radiation of characteristic wavelengths. The emitted gamma-rays are then counted by an HPGe detector placed at a ninety degree angle to the incident neutron beam. Each gamma-ray is counted based on its energy level through the multi-channel analyzer and recorded using Canberra Genie 2000 software.

Both prompt gamma-rays and delayed gamma-rays can be analyzed using this beam port. For prompt gamma-ray analysis, the solid-state detector counts photon emission at the same time the sample is irradiated. Delayed gamma-ray analysis differs in that gamma-ray emission is counted after the sample is irradiated, not simultaneously as in PGAA.

A Boral shutter (a boron-doped aluminum sheet) that connects the reactor pool to the neutron guide is used to stop the neutron beam. In this way, the sample can be irradiated for a period of time ranging from one minute and ten minutes. When the shutter closes and irradiation ceases, gamma-ray counting can proceed. However, the shutter takes almost 2 seconds to close or open completely; meaning that some prompt gamma-ray photons will be recorded in the spectra.

3.2.2 Beam Chopper

A beam chopper was constructed to overcome the delayed opening and closing of the beam port shutter. The beam chopper utilizes a borated aluminum plate with two equally spaced holes. The borated aluminum disk has a 17.5 cm diameter and is 1 mm thick, shown in Figure 3.3 [34].

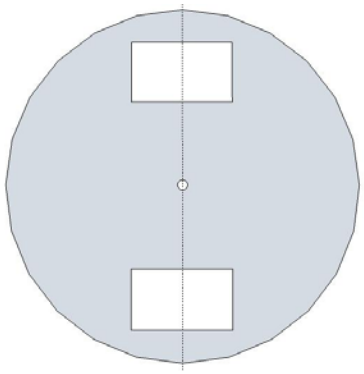

Figure 3.3: The schematic drawing of the borated aluminum plate [34].

The system was modeled after the beam chopper at the Budapest Neutron Center [35], as shown in Figure 3.4. The beam chopper at the Budapest Neutron Center allows for recording both the prompt and delayed spectra while operating [8]. The chopper allows for a faster switch between irradiation of the sample and counting of the gamma-rays, but only records while the sample is not being irradiated. Shorter irradiation and counting times, on the order of fractions of a second, can be achieved using the beam chopper.

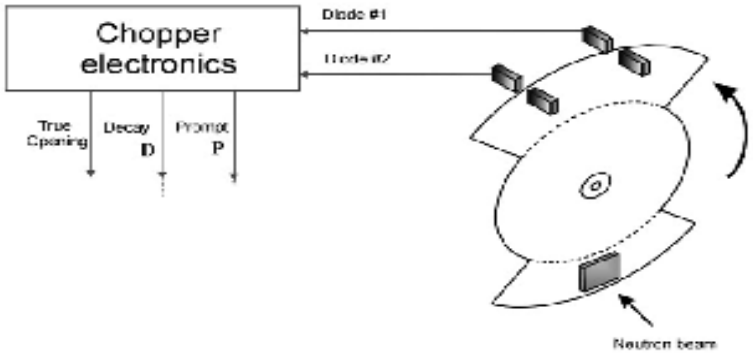

Figure 3.4: Beam chopper at Budapest Neutron Centre [35].

Gamma-ray counting is initialized or halted using a circuit connected to two diode lasers that detect when the shutter is open or close. When the first diode no longer senses that the borated aluminum plate, shown in Figure 3.5 is in place, the circuit sends a pulse to the system to halt data recording. However, when the second laser diode senses that the shutter is in place, gamma-ray counting is restarted. While the chopper system is in place, the circuit continuously sends pulses to the data acquisition system.

Figure 3.5: Picture of the beam chopper stopped in the irradiation phase.

3.3.3 High-Purity Germanium Detectors

The spectra are collected using an HPGe detector. The HPGe is cooled by liquid nitrogen to about 77 K to limit the thermal excitation of electrons into the conduction band, which would otherwise introduce noise into the system. Gamma-ray absorption is the only way for the valence electrons to overcome the large band gap energy. Thus, HPGe detectors usually have highly accurate counting statistics.

Figure 3.6: HPGe and shielding in the PGAA set-up.

The HPGe detector is behind the lead shielding, shown in Figure 3.6, to shield the detector radiation and decrease the noise in the system. The detector is set-up perpendicular to the beam of neutrons to preserve the crystal. The HPGE detector used in the experiment is a p-type crystal geometry and a relative efficiency at 1.33 MeV using a ^{60}Co source of 81.2%.

3.3 SAMPLES

The nuclear materials that need to be detected are widespread. However the samples chosen contain materials that are a proliferation risk. The experiments utilize two samples—a uranium fission chamber and a MOX fuel pellet. The uranium fission

chamber represents a highly enriched uranium sample. The MOX fuel pellet was chosen because of the proliferation risk raised by the reprocessing of spent nuclear fuel.

3.3.1 Fission Chamber

The uranium fission chamber is examined using both the beam chopper method and the on/off method with the beamport shutter. The fission chamber is tall cylinder that is pictured in Figure 3.7. The fission chamber holds a thin layer of highly enriched uranium below the aluminum encasing. One of the major peaks in the prompt and delayed spectrum is the aluminum peak at 1778 keV. The aluminum peak does not represent a fission product and only informs us of the material that encloses the sample. Therefore the peak is ignored in the analysis of the fission product spectra.

Figure 3.7: The aluminum enclosed uranium fission chamber.

3.3.2 MOX fuel pin

The MOX fuel pin is a mixed oxide spent nuclear fuel. The fuel pin is a small cylinder with a tightly packed mixture of spent fuel, as shown in Figure 3.8. The mixed oxide fuel generally refers to a mixture of more than one oxide of fissile or fertile materials. Specifically the MOX fuel contains plutonium oxides and uranium. The uranium in MOX fuel can be reprocessed uranium, depleted uranium or natural uranium. MOX fuel is useful because it can be made with weapons grade plutonium, which decreases the proliferation risk of the plutonium. Plutonium can be easily extracted from spent MOX fuel in countries with reprocessing technology.

Figure 3.8: The MOX fuel pin.

Chapter 4: Results and Discussion

4.1 CALIBRATION

4.1.1 Energy Calibration

The energy calibration for the system was started by counting a ^{152}Eu source for approximately 12 hours while the reactor was off. The sample was recorded at different intervals to check that the system and the electronics were not drifting. The peaks in the spectrum collected were compared to the expected gamma energy values of ^{152}Eu source. The channel of the peak was correlated to the expected energy.

In order to calibrate the system for a larger energy range, a vanadium foil was irradiated and recorded for approximately 6 hours. The vanadium sample produces more prompt gamma-rays than the ^{152}Eu source. The prompt gamma-rays from the vanadium also encompass a larger energy range than the gamma-rays from the ^{152}Eu source. By using the vanadium foil in the energy calibration, the data collection system is calibrated to record gamma-rays up to 7200 keV.

The channel which the gamma-ray was recorded by the data collection system was correlated to the energy of the gamma-ray using the equation derived from the ^{152}Eu source and vanadium samples. A power function is fit to the data collected from the channel of the photopeak and the expected energy of the specific photopeak. The combined vanadium and ^{152}Eu source data is shown in Figure 4.1. The specific equation relating the channel of our data acquisition system to the energy of the gamma-rays recorded is

$$\text{Energy} = -1.3298 * 10^{-12} * \text{Ch}^3 - 3.1169 * 10^{-8} * \text{Ch}^2 + 6.7474 * 10^{-1} * \text{Ch} - 1.4553$$

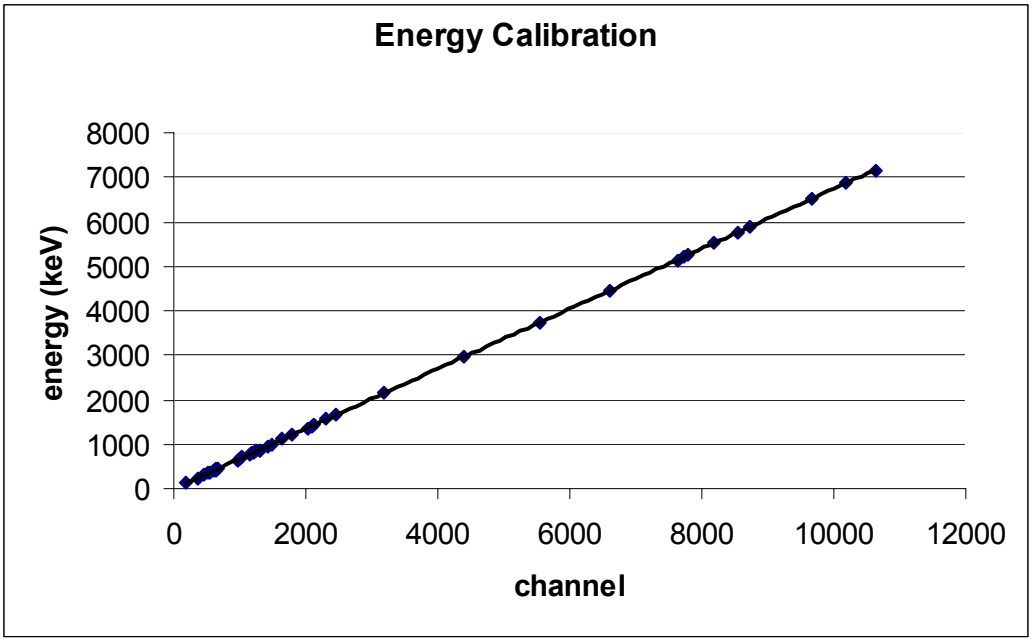

Figure 4.1: The power fit was used by using photopeaks from both the ^{152}Eu source and vanadium foil.

4.1.2 Resolution Calibration

The resolution of the peaks can be established after the energy to channel relationship is quantified. Using the ^{152}Eu source and vanadium foil spectra, the energy level was correlated to the full width half-maximum of each peak. The relationship was described by

$$FWHM = a + b\sqrt{E} \qquad (4.2)$$

where E is the energy of the photopeak, a and b are constants. The full width half-maximum of the photopeaks used in the energy calibration are plotted in Figure 4.2. The relationship between the energy of the gamma-ray and the full width half-maximum of the photopeak is described by the following equation:

$$FWHM = 0.0548 * \sqrt{E} + 0.6245 \quad (4.3)$$

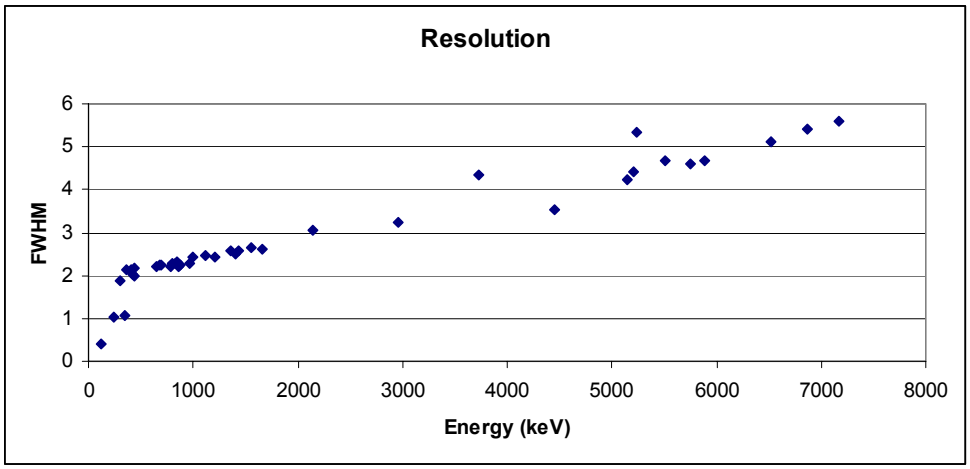

Figure 4.2: The resolution calibration was obtained by using photopeaks from a ^{152}Eu source and vanadium foil.

4.1.3 Efficiency Calibration

The ^{152}Eu source and vanadium foil are also used for the efficiency calibration of the system. By calculating the activity of the ^{152}Eu source, the number of gamma-rays released per energy level can be calculated using the absolute yield and the counting time. The actual number of gamma-rays at a specific energy level is divided over expected number of gamma-rays at that energy level to give the efficiency of the detector at that energy level. The efficiency is calculated for each of the expected photopeaks for ^{152}Eu source and a curve is fit to the data. Equation (2.7) can be rearranged to calculate the efficiency of the detector at the ^{152}Eu photopeaks.

$$\varepsilon = \frac{counts}{A \cdot t \cdot \gamma_i} \quad (4.4)$$

Using a vanadium photopeak that falls between two similar energy gamma-rays from the ^{152}Eu source, the efficiency of the detector at the energy level of the vanadium

photopeak is found through linear extrapolation. By rearranging equation (4.4), the activity for vanadium foil is calculated. Using the calculated activity and equation (4.4), the detector efficiency is extrapolated to 7200 keV.

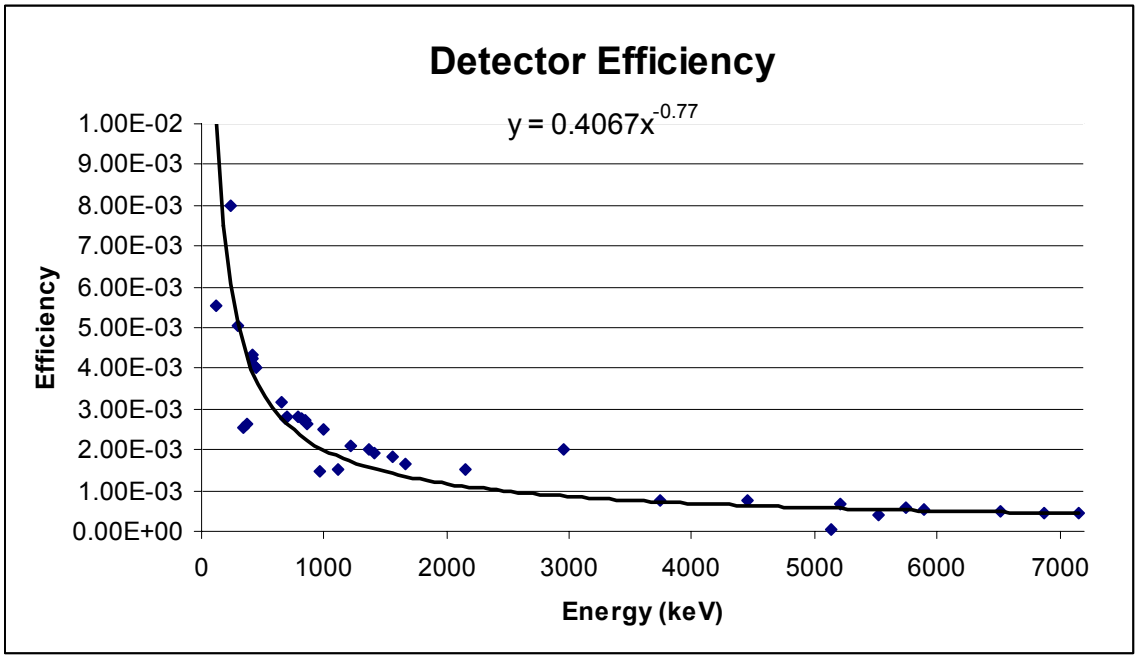

Figure 4.3: The detector efficiency utilizing the ^{152}Eu source and vanadium foil spectra.

4.2 PROMPT GAMMA-RAYS

The MOX fuel pellet is a dense sample, which exhibits self-shielding. The self-shielding of the sample, an attribute of plutonium and uranium, is noticeable in both the prompt and delayed spectra. The MOX sample produces a smooth line with no major photopeaks when counted during irradiation, as shown in Figure 4.4. The smooth prompt spectrum is similar to the delayed spectrum even when recorded for hours after irradiation. A more in-depth study of the data collected using the MOX fuel pellet should be considered.

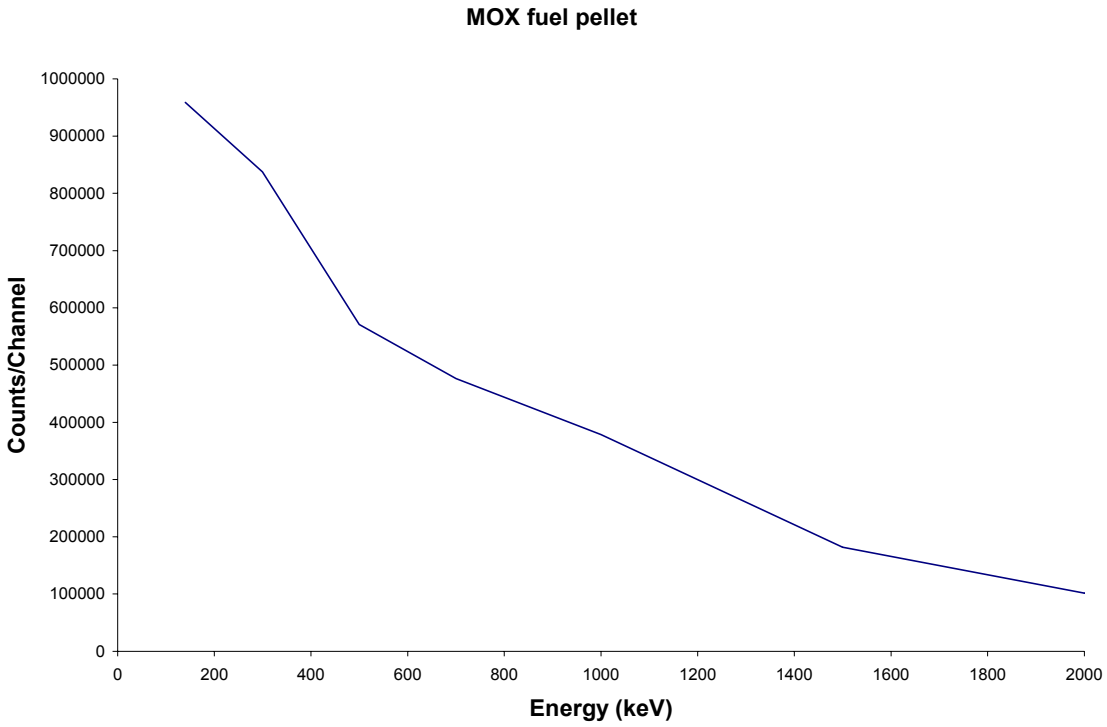

Figure 4.4: The prompt spectrum of the MOX fuel pellet. Counting time was 1 hour.

The MOX fuel pellet data can also be compared to the plutonium data collected by Verbinkski, Weber, and Sund [17]. The empirical relationships expressed in equations (2.10) and (2.11) [18, 30] are for uranium samples, but both relationships are frequently used for other nuclear materials like ^{239}Pu and ^{252}Cf. As shown in Figure 4.5, both of the empirical relationships fit the MOX fuel pellet data well. The Verbinski, Weber, and Sund data is collected for a ^{239}Pu source [17]. Therefore, it is not surprising that the data differs from the data collected from our MOX fuel pellet sample.

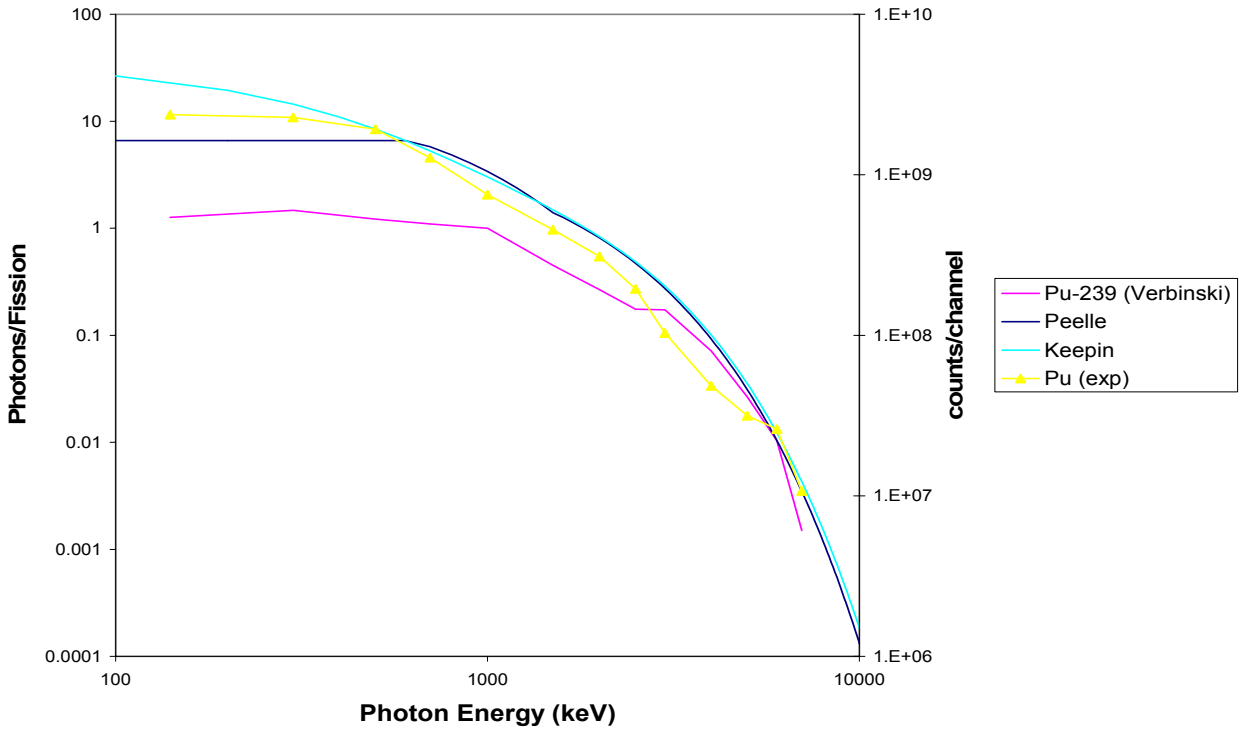

Figure 4.5: The experimental data collected by Verbinski, Weber, and Sund [17] is compared to the data from the MOX fuel pellet. The empirical relationships expressed in equations (2.10) and (2.11) are compared to the plutonium data.

The highly enriched uranium source has a few peaks attributed to prompt gamma-rays during irradiation. The spectrum, shown in Figure 4.6, shows the spectrum of the uranium sample that was counted during the irradiation of the sample. The aluminum peak at 1778 keV was removed from the spectrum because it overwhelmed the rest of the peaks.

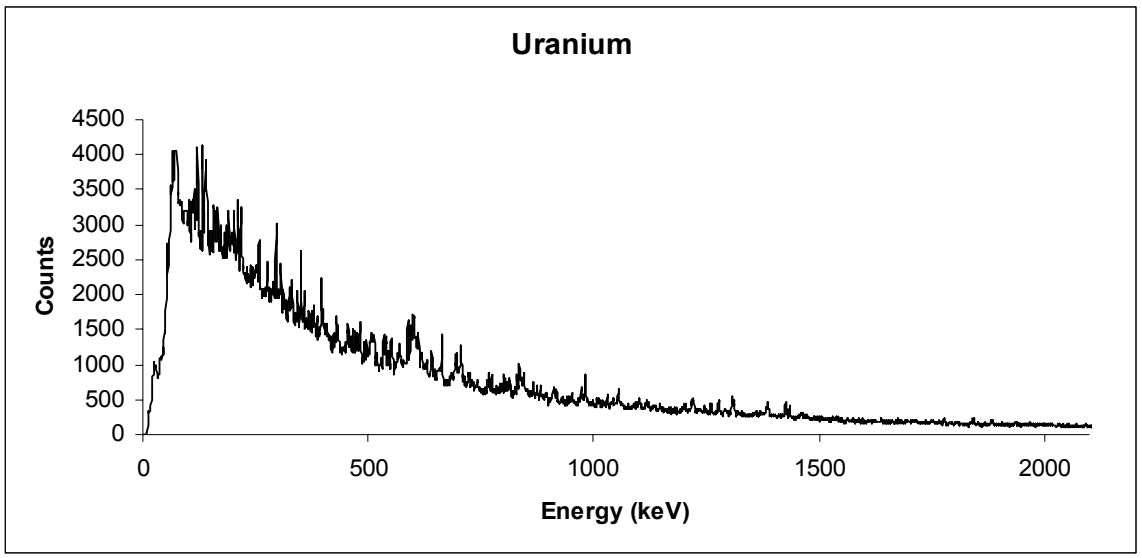

Figure 4.6: The prompt spectrum of a highly enriched uranium source.

The spectrum from the highly enriched uranium sample matched the data collected by Verbinski, Weber, and Sund, which also was collected using a highly enriched uranium foil [17] and the two empirical relationships expressed in equations (2.10) and (2.11). Figure 4.7 shows the binned uranium data in comparison to the published data and empirical formulas also show a similar shape.

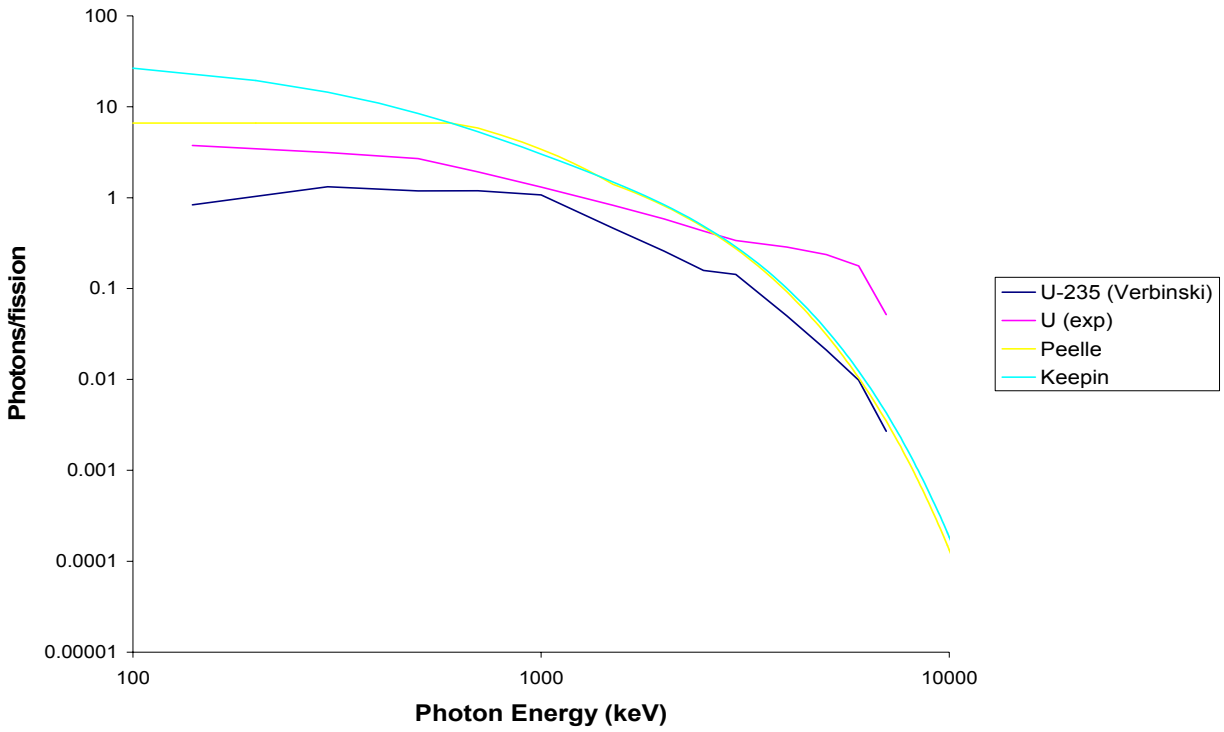

Figure 4.7: The highly enriched uranium data is shown in contrast to other experimentally collected data [17] and two empirical fits [18, 30].

4.3 DELAYED GAMMA-RAYS

There were two methods used to capture the delayed gamma-rays of the short lived fission products created in the samples. The first was the on and off method, which allowed the sample a counting time of one minute to five minutes after irradiation. The beam chopper was used for shorter time intervals. The beam chopper allowed the examination of delayed gamma-rays of fission products with short lived half lives.

The fission chamber was irradiated for approximately one hour to allow the build-up of fission products in the sample. The spectrum shown in Figure 4.8 displays the results from the uranium sample recorded for approximately one second after approximately half a second of irradiation. This cycle of irradiation on/counting off and

counting on/irradiation off continued for approximately two hours. The large peak at 1778 keV from the aluminum casing was subtracted out of the spectra to showcase the peaks due to the fission products.

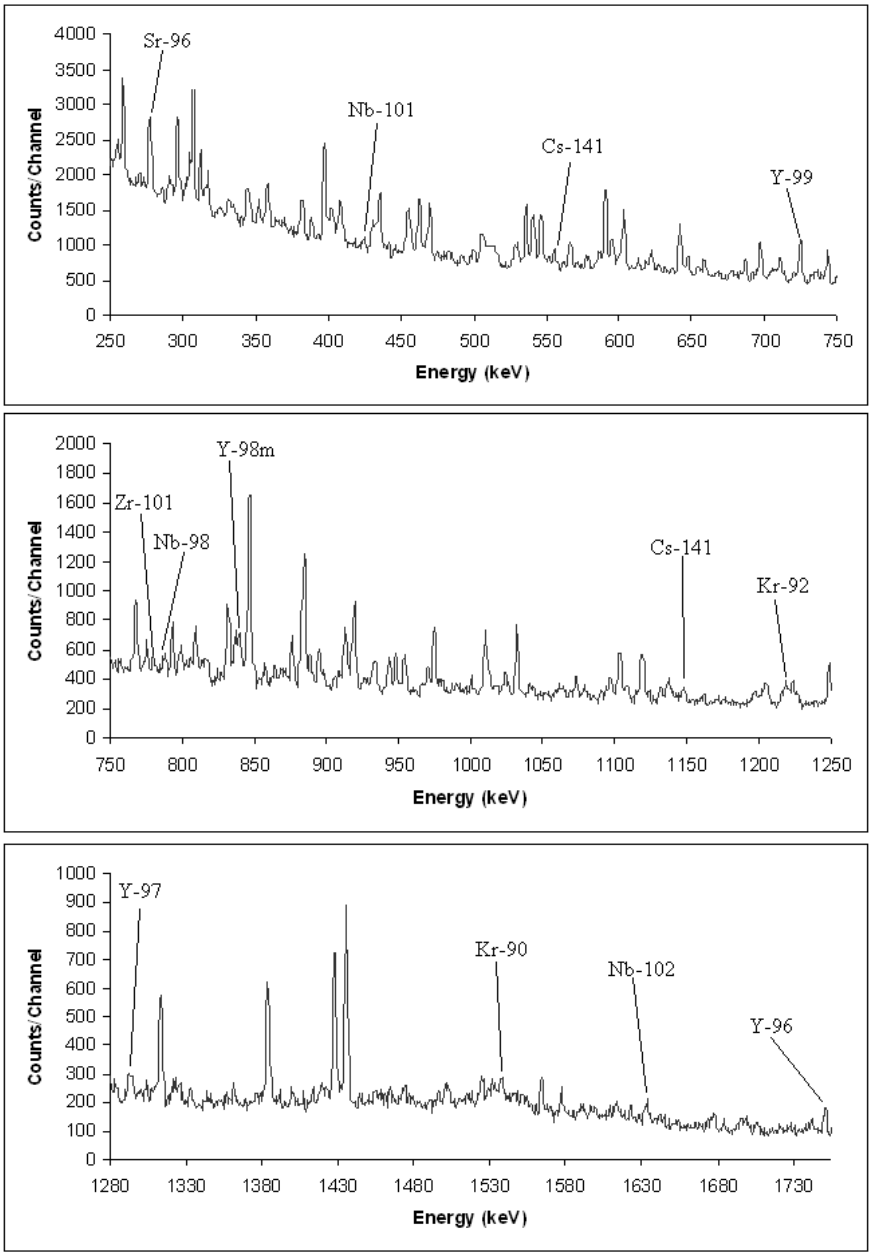

Figure 4.8: The uranium sample with a cycle of half a second in the beam followed by 1 second of counting. The spectrum was collected over a 2 hour period.

The peaks from the spectrum were identified and gamma-ray production for fission products were examined. The gamma-rays from the fission products were assigned to the different peaks. The majority of the peaks are composed of gamma-rays from multiple nuclides. The full spectrum and photopeak identification are shown in Table 4.1. Appendix A has a similar table with the classification of the energy peaks by nuclide. There were 27 peaks attributed to gamma-rays from a single nuclide. Only 7 of the single nuclide peaks are also in the prompt spectrum of the uranium sample.

Table 4.1: The list of peaks by energy and the fission products that have gamma-rays that comprise the peak for the data collected using the beam chopper method.

Energy (keV)	**Nuclides**
107.35	^{138m}Cs, ^{103}Y
120.52	^{99}Sr, ^{140}Xe, ^{103}Zr, ^{147}La, ^{96}Sr, ^{99}Y, ^{100}Y, ^{99}Kr
136.25	^{102}Mo, ^{94}Kr
138.73	^{103}Nb, ^{105}Nb
142.55	^{92}Kr, ^{79}Ga, ^{74}Zn, ^{124}Cd
149.26	^{103}Y, ^{105}Nb, ^{102}Sr, ^{102}Mo, ^{103}Zr, ^{103}Y
164.17	^{145}La, ^{103}Zr, ^{157}Pm, ^{152}Pr, ^{115}Rh, ^{101}Sr, ^{154}Pr
175.83	^{80}Zn, ^{145}Cs, ^{160}Eu
186.44	^{94}Kr, ^{147}La
191.6	^{142}Xe, ^{111}Rh, ^{153}Pr, ^{105}Nb, ^{94}Kr, ^{143}Cs, ^{108}Nb
206.07	^{101}Zr, ^{109}Ru
211.86	^{111}Ru, ^{113}Ru, ^{102}Mo, ^{140}Xe, ^{100}Y, ^{143}Ba, ^{93}Rb
219.33	^{93}Rb, ^{94}Kr
232.41	^{143}Cs, ^{105}Nb

Table 4.1 continued: The list of peaks by energy and the fission products that have gamma-rays that comprise the peak for the data collected using the beam chopper method.

242.94	^{87}Se, ^{137}Te, ^{145}Cs, ^{110}Tc, ^{90}Kr, ^{108}Tc
255.65	^{102}Sr, ^{153}Nd
259.26	^{88}Se, ^{103}Y, ^{80}Ge
277.61	^{96}Sr
296.99	^{102}Nb, ^{97}Y
307.5	^{97}Sr, ^{146}Cs, ^{105}Nb, ^{111}Ru, ^{83}Ge
312.87	^{80}Zn, ^{121}Ag
317.23	^{114}Rh, ^{94}Kr, ^{92}Kr
345.34	^{153}Nd, ^{85}Se, ^{91}Rb
352.39	^{95}Rb, ^{145}La, ^{121}Ag
358.58	^{142}Cs, ^{102}Mo, ^{145}La, ^{94}Kr, ^{137}Te, ^{109}Ru
382.05	^{111}Ru, ^{86}Se
388.55	^{115m}Ag, ^{112}Rh, ^{144}Ba, ^{99}Zr
398.03	^{116}Rh, ^{102}Nb, ^{91}Kr
402.54	^{117}Pd, ^{102}Nb
408.37	^{112}Tc, ^{88}Se
417.6	^{145}Ba, ^{97}Rb, ^{153}Nd
424.62	^{110}Tc, ^{109}Ru
431.54	^{76}Cu, ^{75}Zn, ^{143}Ba, ^{144}Ba, ^{93}Rb
435.26	^{145}Cs, ^{125}Cd
440.99	^{101}Nb
455.24	^{103}Nb, ^{145}Cs
462.99	^{116}In, ^{128}Cd, ^{101}Sr, ^{80}Zn, ^{124}Ag, ^{106}Mo, ^{99}Zr,
469.44	^{99}Zr, ^{137}Te, ^{87}Se
499.97	^{121}Ag, ^{100}Zr, ^{103}Tc
505.58	^{120}Ag, ^{103}Nb, ^{91}Kr, ^{106}Mo

Table 4.1 continued: The list of peaks by energy and the fission products that have gamma-rays that comprise the peak for the data collected using the beam chopper method.

529.84	^{96}Sr, ^{81}Ga
535.99	^{99}Y, ^{88}Sr, ^{123}In, ^{124}Ag
541	^{112}Rh, ^{141}Xe, ^{144}Ba, ^{90}Kr
546.76	^{145}Cs, ^{99}Zr, ^{92}Kr
551.58	^{102}Nb, ^{137}Te
555.73	^{141}Cs
566.57	^{80}Zn, ^{140}I, ^{78}Ga
578.43	^{95}Rb, ^{99}Y
586.1	^{80}Ga, ^{141}Cs, ^{108}Nb
590.62	^{108}Nb, ^{101}Sr
595.57	^{96}Sr, ^{106}Mo, ^{94}Kr
602.87	^{99}Y, ^{137}Te
613.52	^{99}Y, ^{80}Zn, ^{100}Y, ^{91}Kr, ^{124}Ag
622.05	^{100}Nb, ^{98m}Y, ^{140}Xe
642.01	^{80}Zn, ^{103}Nb
647.72	^{98m}Y, ^{98}Nb
654.06	^{102}Nb, ^{97}Sr, ^{82}As, ^{140}Xe
658.61	^{135}Sb, ^{80}Ga, ^{143}Cs
686.46	^{80}Zn, ^{117m}Ag, ^{95}Sr, ^{97}Rb, ^{126}Cd
691.84	^{96}Rb, ^{141}Cs
697.37	^{120}Ag, ^{97}Sr, ^{94}Kr
710.75	^{81}Ga, ^{137}Te, ^{80}Zn, ^{87}Se, ^{93}Rb
724.7	^{99}Y
735.76	^{80}Zn, ^{146}Cs
743.26	^{80}Zn, ^{102}Y, ^{123}Ag, ^{116}Rh
751.08	^{98m}Y, ^{145}Cs

Table 4.1 continued: The list of peaks by energy and the fission products that have gamma-rays that comprise the peak for the data collected using the beam chopper method.

767.89	^{100}Nb, ^{94}Kr, ^{129}In
775.48	^{88}Br, ^{140}Xe
780.94	^{101}Zr
787.86	^{98}Nb
793.85	^{154}Pr, ^{81}Ge
799.39	^{97}Sr, ^{88}Br, ^{143}Ba
809.51	^{96}Sr, ^{140}Xe
816.14	^{120}Ag, ^{92}Rb, ^{96}Rb, ^{121}Ag
824.93	^{160}Eu, ^{90m}Rb, ^{95}Sr
832.03	^{90}Rb, ^{90m}Rb
837.07	^{94}Rb, ^{124}Ag
840.24	^{98m}Y
847.2	^{102}Nb, ^{111}Ru
857.55	^{128}Cd, ^{133}In
864.62	^{100}Y
876.46	^{92}Kr, ^{100}Y
888.63	^{109}Ru, ^{155}Nd
895.3	^{154}Pr, ^{143}Ba, ^{137}Te
913.5	^{136m}I, ^{101}Zr
919.18	^{96}Y, ^{121}In
933.27	^{146}Cs, ^{154}Pr, ^{96}Sr, ^{80}Ge
943.72	^{95}Sr
948.67	^{122}In, ^{102}Nb
953.89	^{97}Sr, ^{89}Br
970.06	^{100}Nb, ^{124}In
1000.99	^{101}Sr, ^{160}Eu, ^{89}Br

Table 4.1 continued: The list of peaks by energy and the fission products that have gamma-rays that comprise the peak for the data collected using the beam chopper method.

1010.4	^{143}Ba, ^{80}Ge, ^{80}Ga, ^{109}Ru, ^{129}In
1032.29	^{125}In, ^{102}Sr
1079.08	^{82}As, ^{144}Cs
1096.8	^{89}Br, ^{100}Y
1103.33	^{97}Y, ^{102}Sr
1118.82	^{108}Tc, ^{90}Kr, ^{80}Ge, ^{144}Cs
1131.8	^{123}In, ^{124}In
1137.26	^{129}In, ^{140}Xe
1147.77	^{141}Cs
1218.45	^{92}Kr
1223.64	^{98}Y, ^{98m}Y, ^{110}Tc
1260.58	^{95}Rb, ^{97}Sr
1268.39	^{135}Sb, ^{111}Ru
1278.85	^{134}Sb, ^{95}Sr, ^{142}Cs, ^{100m}Nb
1293.62	^{97}Y, ^{95}Sr
1304.51	^{87}Se, ^{109}Ru, ^{160}Eu
1313.31	^{80}Ga, ^{136m}I, ^{136}I, ^{240}Xe
1333.17	^{124}Ag, ^{80}Zn, ^{125}In
1384.13	^{92}Rb, ^{160}Eu, ^{93}Rb
1391.5	^{110}Tc, ^{122}In, ^{86}Br
1400.14	^{97}Y, ^{111}Ru
1413.82	^{140}Xe, ^{110}Tc, ^{83}Ge
1428.01	^{94}Sr, ^{85}Se
1435.96	^{83}Ge, ^{138m}Cs
1501.93	^{100}Nb, ^{91}Kr, ^{80}Zn, ^{109}Ru
1525.05	^{83}Ge, ^{144}La

Table 4.1 continued: The list of peaks by energy and the fission products that have gamma-rays that comprise the peak for the data collected using the beam chopper method.

1537.72	^{90}Kr
1564.63	^{80}Ge, ^{133}In
1577.4	^{94}Rb, ^{88}Br, ^{110}Tc
1633.19	^{102}Nb
1677.91	^{80}Ga, ^{104}Tc, ^{77m}Ge
1750.77	^{96}Y
1806.68	^{110}Tc, ^{95}Y, ^{93}Rb
1835.81	^{135}Sb, ^{98}Rb
1904.35	^{97}Sr
1970.91	^{82}As, ^{91}Rb, ^{146}Cs
2005.19	^{133}In, ^{87}Br
2015.6	^{144}Cs
2175.61	^{144}Cs
2196.02	^{83}Ge, ^{89}Rb
2289.46	^{136}I
2392.17	^{120}In
2415.64	^{136}I
2441.73	^{100}Y, ^{81}Ga
2570.18	^{135}Sb, ^{89}Rb
2590.69	^{91}Kr
2631.28	^{134}Sb
2639.33	^{100}Y
2717.38	^{95}Sr
2752.73	^{86}Br, ^{91}Kr
2820.86	^{92}Rb
2942.49	^{98}Y

Table 4.1 continued: The list of peaks by energy and the fission products that have gamma-rays that comprise the peak for the data collected using the beam chopper method.

2960.46	^{136}I
3287.48	^{97}Y
3400.9	^{97}Y, ^{85}Se
3599.63	^{91}Rb
4019.91	^{93}Rb
4134.49	^{90}Rb
4642.49	^{92}Rb, ^{90}Rb

The spectrum, shown in Figure 4.9, shows the uranium sample counted for one minute while the shutter was closed and irradiated for one minute between counting. Since the beam port shutter takes approximately 2 seconds to completely close or open, the fission products with extremely short half lives are not able to be examined using this method. The large peak at 1778 keV ignored in the data analysis because it is due to the aluminum casing of the sample.

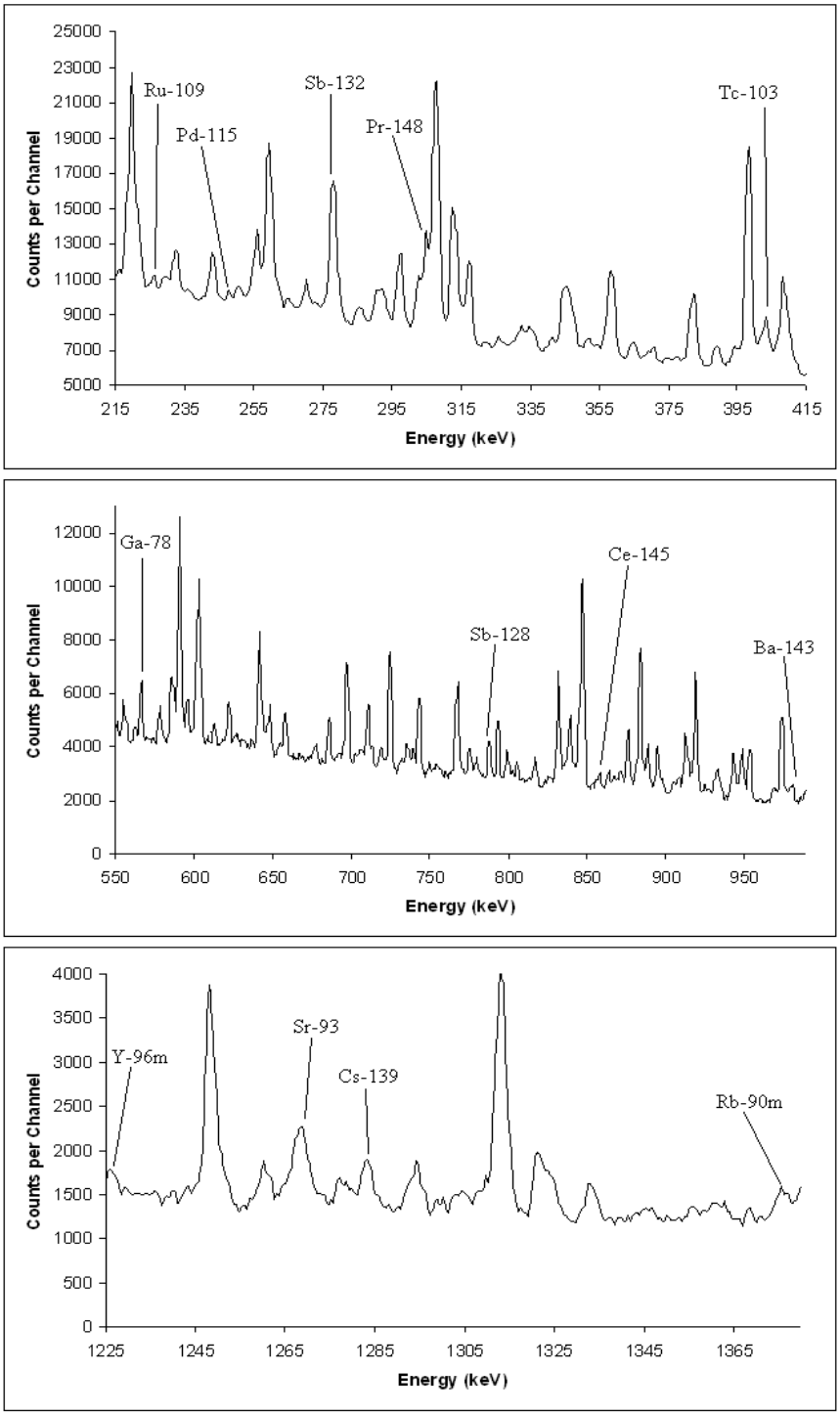

Figure 4.9: The uranium sample with an irradiation time of one minute and a counting time of one minute.

The full list of peaks in the spectra are listed in Table 4.2 The fission products with cumulative yields above 10^{-4} and gamma yields above 1% absolute yield were considered. The nuclides that comprise each peak are listed in the table. There are 62 peaks in the on/off fission chamber spectrum that are attributed to a single nuclide. A table containing the peak energy by nuclide is in Appendix B.

Table 4.2: The list of peaks by energy and the fission products that have gamma-rays that comprise the peak for the data collected using the on/off method.

Energy (keV)	**Nuclides**
87.35	^{151}Nd ^{155}Nd ^{149}Ce
92.14	^{91}Rb ^{116}Pd ^{145}Ba ^{81}Ge
96.76	^{99m}Nb ^{159}Eu ^{113}Pd ^{145}Ba
102.52	^{132}Sb ^{148}Ce
107.82	^{91}Kr ^{153}Nd ^{149}Pr
120.39	^{90}Kr ^{140}Xe ^{148}Ce
136.67	^{117m}Ag ^{117}Ag ^{103}Tc
139.23	^{151}Nd ^{149}Pr
144.04	^{96m}Y ^{159}Eu ^{149}Ce
150.39	^{132}Sb ^{130}Sn
157.31	^{117m}Ag ^{117}Ag
163.94	^{145}Ba ^{145}La
166.35	^{149}Pr ^{134}Sb
169.1	^{93}Sr ^{151}Nd
175.63	^{160}Eu ^{156}Pm ^{75}Ga
182.35	^{130m}Sb ^{155}Nd ^{146}La
186.29	^{155}Nd

Table 4.2 continued: The list of peaks by energy and the fission products that have gamma-rays that comprise the peak for the data collected using the on/off method.

190.87	^{138m}Cs	^{101}Mo	^{130}Sn	^{145}Ba
192.75	^{138m}Cs	^{101}Mo	^{130}Sn	^{128}Sb
197.69	^{136m}I	^{157}Sm		
205.94	^{117m}Ag	^{109}Ru		
211.45	^{143}Ba	^{103}Tc		
219.43	^{117m}Ag	^{89}Kr	^{129m}Sn	^{155}Nd
225.87	^{109}Ru			
232.13	^{142}Ba	^{145}Ce		
242.81	^{138}Xe	^{90}Kr	^{152m}Pm	^{87}Se
247.47	^{115}Pd			
250.67	^{75}Ga	^{120}In		
255.61	^{142}Ba	^{143}Ba	^{151}Nd	
259.11	^{138}Xe	^{93}Sr	^{121}In	^{146}La
264.63	^{80}Ge	^{129m}Sn		
270.01	^{106}Tc	^{148}Ce	^{113}Pd	
277.82	^{132}Sb			
285.5	^{145}Ce	^{153}Nd		
291.23	^{143}Ba	^{132}Sb	^{146}La	^{148}Ce
297.08	^{117m}Ag	^{134}Sb		
302.22	^{148}Pr			
304.59	^{115}Pd			
307.37	^{117m}Ag	^{142}Ba	^{129m}Sn	
312.62	^{117}Ag	^{128}Sb		
317.03	^{149}Pr	^{157}Sm		

Table 4.2 continued: The list of peaks by energy and the fission products that have gamma-rays that comprise the peak for the data collected using the on/off method.

325.69	^{148}Ce	^{109}Rh		
333.93	^{87}Se	^{149}Pr		
344.41	^{85}Se	^{153}Nd	^{103}Tc	^{115}Pd
346.33	^{91}Rb	^{136m}I	^{93}Sr	^{103}Tc
351.86	^{99m}Nb	^{145}Ce	^{148}Ce	
358.12	^{104}Tc	^{109}Ru	^{83}Se	
364.54	^{96m}Y	^{142}Ba		
369.84	^{136m}I	^{110}Rh	^{130m}Sb	
381.87	^{136m}I	^{86}Se	^{132}Sb	^{145}Ba
388.8	^{103}Tc	^{81}As		
394.07	^{157}Sm	^{137}Xe		
397.81	^{91}Kr	^{138}Xe	^{144}La	^{115}Pd
402.79	^{103}Tc			
408.14	^{101}Mo	^{155}Pm	^{146}La	
417.78	^{153}Nd	^{145}Ba	^{155}Nd	
424.62	^{109}Ru	^{142}Ba	^{145}Ce	^{151}Nd
431.31	^{95}Y	^{85}Se	^{143}Ba	
435.05	^{138}Xe	^{143}Ba	^{130}Sn	
440.23	^{91}Rb	^{145}Ce	^{110}Rh	
451.32	^{99m}Nb	^{148}Pr		
455.25	^{137}Xe	^{146}La	^{143}La	
462.88	^{138m}Cs	^{113}Pd		
468.25	^{117}Ag	^{81}As	^{130m}Sb	^{87}Se
475.56	^{102}Tc	^{153}Nd		

Table 4.2 continued: The list of peaks by energy and the fission products that have gamma-rays that comprise the peak for the data collected using the on/off method.

482.96	^{136m}I	^{113}Pd		
492.26	^{81}As	^{74}Ga	^{145}Ba	
498.76	^{101}Mo	^{89}Kr	^{132}Sb	^{130m}Sb
506.1	^{91}Kr	^{101}Mo	^{129m}Sn	
530.09	^{87}Br	^{104}Tc		
535.83	^{99m}Nb	^{104}Tc		
540.97	^{90}Kr	^{144}La	^{100}Tc	
546.64	^{110}Rh	^{154}Pm	^{138}Cs	^{145}Ba
551.1	^{130}Sn	^{102}Nb		
555.42	^{91}Kr	^{90}Kr	^{140}Xe	^{141}Cs
562.07	^{141}Cs	^{103}Tc	^{76}Ga	
566.43	^{78}Ga			
578.31	^{75}Ga	^{68}Cu	^{129}Sn	
586.06	^{89}Kr	^{144}La	^{151}Nd	^{141}Cs
590.6	^{101}Mo	^{93}Sr	^{100}Tc	
595.92	^{91}Rb	^{74}Ga		
602.78	^{91}Rb	^{140}Cs	^{129m}Sn	
607.92	^{101}Mo	^{74}Ga	^{85}Se	^{140}Xe
613.15	^{91}Kr	^{148}Pr		
621.86	^{140}Xe	^{143}La	^{78}Ga	
627.09	^{139}Cs	^{102}Tc		
631.37	^{99m}Nb	^{102}Tc		
636.44	^{148}Pr	^{132}Sb	^{102}Tc	^{120}In
641.89	^{101}Mo	^{131}Sb	^{143}La	

Table 4.2 continued: The list of peaks by energy and the fission products that have gamma-rays that comprise the peak for the data collected using the on/off method.

647.54	^{129}Sn	^{130m}Sb		
658.12	^{89}Rb	^{148}Pr	^{121}In	^{131}Sb
667.2	^{80}As	^{146}La		
677.3	^{151}Nd	^{159}Eu		
686.02	^{95}Sr	^{117m}Ag		
697.2	^{101}Mo	^{148}Pr	^{132}Sb	
710.55	^{93}Sr	^{134}Sb		
719.65	^{148}Pr	^{143}Ba	^{83}Se	
724.46	^{145}Ce	^{155}Pm		
735.7	^{83}As	^{144}La	^{151}Nd	
739.11	^{89}Kr	^{151}Nd		
743.17	^{128}Sb	^{130}Sn		
775.41	^{88}Br	^{140}Xe		
780.15	^{152m}Pm	^{130}Sn	^{155}Pm	
787.76	^{128}Sb			
793.64	^{130m}Sb	^{81}Ge		
799	^{143}Ba	^{151}Nd	^{83}Se	
805.62	^{85}Br	^{88}Br	^{140}Xe	^{159}Eu
816.88	^{133}Sb	^{132}Sb	^{130m}Sb	
831.79	^{90}Rb	^{87}Br	^{90m}Rb	
839.66	^{85}Se	^{142}Ba	^{110}Rh	^{130m}Sb
846.89	^{144}La	^{102}Nb		
857.57	^{145}Ce			
864.13	^{120}In	^{85}Br	^{102}Tc	

Table 4.2 continued: The list of peaks by energy and the fission products that have gamma-rays that comprise the peak for the data collected using the on/off method.

867.86	^{74}Ga ^{89}Kr
871.36	^{101}Mo ^{138m}Cs ^{138}Cs
876.16	^{93}Sr ^{81}Ge
884.16	^{104}Tc ^{75}Ga
888.61	^{93}Sr ^{83}Se
895.18	^{104}Tc ^{142}Ba ^{143}Ba
904.96	^{89}Kr ^{110}Rh
908.55	^{140}Cs ^{121m}In
913.26	^{136m}I ^{96m}Y
918.88	^{85}Br ^{121}In
925.5	^{140}Xe ^{143}Ba ^{121}In ^{146}La
933.03	^{101}Mo ^{80}Ge ^{156}Pm ^{131}Sb
943.44	^{87}Br ^{85}Se ^{131}Sb
948.48	^{91}Rb ^{89}Rb ^{142}Ba
953.62	^{95}Y ^{85}Se ^{155}Nd
969.43	^{154}Pm ^{153}Nd
974.43	^{89}Kr ^{132}Sb
980.07	^{143}Ba
989.88	^{140}Xe ^{83m}Se ^{157}Sm
1000.95	^{74}Ga ^{142}Ba
1010.12	^{101}Mo ^{109}Ru ^{143}Ba
1017.52	^{90}Kr ^{151}Nd ^{130m}Sb
1023.72	^{87}Br ^{91}Kr
1031.92	^{89}Rb ^{83m}Se

Table 4.2 continued: The list of peaks by energy and the fission products that have gamma-rays that comprise the peak for the data collected using the on/off method.

1041.14	^{91}Rb	^{121}Cd	^{128}Sb	^{121m}In
1061.08	^{90}Rb	^{90m}Rb		
1078.62	^{68}Cu	^{142}Ba		
1095.89	^{133}Sb	^{142}Ba	^{152m}Pm	
1102.73	^{91}Kr	^{102}Tc	^{121m}In	
1108.07	^{91}Kr	^{96m}Y	^{89}Kr	^{145}Ce
1118.44	^{86}Se	^{80}Ge	^{121m}In	
1123.8	93Sr	^{151}Nd	^{131}Sb	
1131.19	^{129m}Sn			
1137.38	^{91}Rb	^{91}Kr	^{140}Xe	
1147.43	^{156}Pm	^{154}Pm	^{145}Ce	^{141}Cs
1160.78	^{101}Mo	^{128}Sb	^{129m}Sn	
1196.96	^{102}Tc	^{143}Ba	^{129}Sn	^{141}Cs
1203.49	^{74}Ga	^{85}Se	^{100}Tc	^{142}Ba
1217.55	^{86}Br			
1225.39	^{96m}Y			
1248.24	^{89}Rb	^{75}Ga	^{148}Pr	
1260.33	^{68}Cu	^{80}Ge	^{156}Pm	
1268.26	^{93}Sr			
1277.79	^{95}Sr	^{86}Se	^{134}Sb	
1283.03	^{139}Cs			
1293.97	^{102}Tc	^{80}As		
1304.6	^{133}Sb	^{101}Mo	^{109}Ru	
1312.92	^{136}I	^{136m}I	^{140}Xe	

Table 4.2 continued: The list of peaks by energy and the fission products that have gamma-rays that comprise the peak for the data collected using the on/off method.

1322.1	^{136}I ^{95}Y ^{89}Kr
1333.03	^{83}As ^{74}Ga
1375.98	^{90m}Rb
1383.75	^{88}Rb ^{160}Eu
1413.86	^{87}Br ^{140}Xe
1420.16	^{87}Br ^{139}Cs
1427.55	^{85}Se ^{94}Sr
1435.52	^{138}Cs ^{138m}Cs ^{152m}Pm
1464.84	^{86}Br ^{157}Sm
1473.23	^{89}Kr
1501.63	^{89}Kr ^{109}Ru
1524.66	^{144}La
1532.07	^{101}Mo ^{89}Kr
1537.4	^{89}Rb ^{90}Kr ^{109}Ru
1551.15	^{133}Sb
1564.39	^{86}Br ^{80}Ge
1577.8	^{87}Br ^{88}Br
1597.82	^{101}Mo ^{104}Tc
1613.95	^{91}Rb ^{137}Xe ^{102}Tc ^{104}Tc
1634.09	^{102}Nb ^{140}Cs
1664.89	^{90m}Rb
1676.84	^{68}Cu ^{104}Tc
1694.07	^{89}Kr
1698.31	^{93}Sr

Table 4.2 continued: The list of peaks by energy and the fission products that have gamma-rays that comprise the peak for the data collected using the on/off method.

1727.66	^{133}Sb ^{85}Br
1740.44	^{91}Rb ^{136m}I
1750.34	^{96m}Y
1756.5	^{109}Ru
1768.1	^{138}Xe
1806.48	^{95}Y
1835.93	^{87}Br ^{88}Rb ^{109}Ru
1851.57	^{91}Rb ^{140}Cs
1901.63	^{89}Kr
1939.32	^{95}Y ^{74}Ga ^{89}Kr
1970.49	^{91}Rb ^{106}Tc ^{144}La
1996.42	^{117}Ag
2004.88	^{87}Br ^{138}Xe
2014.88	^{138}Xe ^{117}Ag
2031.25	^{101}Mo
2040.01	^{101}Mo
2077.84	^{83}As
2100.9	^{140}Cs ^{81}As ^{89}Kr
2127.47	^{90m}Rb
2174.96	^{95}Y
2195.38	^{89}Rb
2217.31	^{138}Cs
2237.62	^{86}Se ^{99m}Nb ^{140}Cs ^{106}Tc
2246.74	^{95}Sr ^{117}Ag ^{102}Tc

Table 4.2 continued: The list of peaks by energy and the fission products that have gamma-rays that comprise the peak for the data collected using the on/off method.

2252.39	^{138}Xe
2289.45	^{136}I
2330.21	^{140}Cs
2349.58	^{86}Br ^{139}Cs
2414.95	^{136}I ^{133}Sb
2441.68	^{86}Se
2483.67	^{91}Kr ^{84}Br
2521.62	^{140}Cs
2542.75	^{99m}Nb
2563.72	^{91}Rb
2569.43	^{89}Rb
2631.82	^{95}Y
2639.2	^{99m}Nb
2662.02	^{86}Se
2706.02	^{87}Br ^{89}Rb
2716.05	^{95}Sr
2751.87	^{90m}Rb ^{86}Br
2849.58	^{137}Xe ^{99m}Nb
2866.6	^{136}I ^{89}Kr
2924.75	^{91}Rb
2932.67	^{95}Sr
2997.22	^{87}Br
3112.55	^{91}Kr
3303.51	^{90}Rb

Table 4.2 continued: The list of peaks by energy and the fission products that have gamma-rays that comprise the peak for the data collected using the on/off method.

3316.31	^{90m}Rb
3382.57	^{90}Rb
3533.57	^{90}Rb ^{89}Kr
3575.06	^{95}Y
3599.05	^{91}Rb
3927.61	^{84}Br
4077.14	^{91}Rb ^{95}Sr
4134.45	^{90}Rb
4180.23	^{87}Br
4364.94	^{90}Rb
4645.76	^{90}Rb

The MOX fuel pellet was irradiated for about 30 minutes to allow the fission products to build-up during the sample. During the longer irradiation, the sample was not counted. After the fission products were allowed to build-up, the shutter was closed, the irradiation was halted, and the counting started. Figure 4.10 shows the spectrum of the sample counted for two hours following the sample irradiation. The MOX fuel pellet spectra were very similar for the beam chopper, on/off method for various times between one and five minutes, and the decay released 2 hours after irradiation.

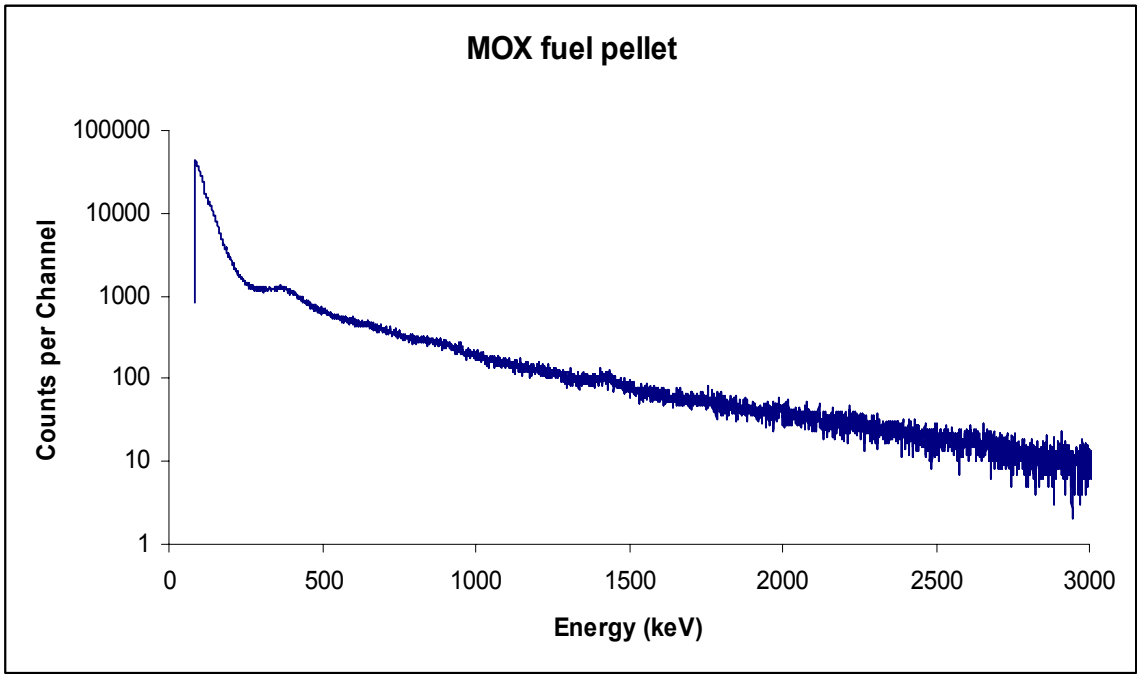

Figure 4.10: The delayed spectra of the MOX fuel pellet.

4.4 ORIGEN

ORIGEN-ARP [36] was used to calculate the fission products that have the highest activity in the spectrum during several different time scenarios—1 second, 10 seconds, 1 minute, 1 hour and 8 hours after irradiation. Using ORIGEN-ARP, a small sample of ^{235}U was irradiated. The concentrations of fission products were recorded based on the amount of time the sample was recorded during decay.

The fission products were ordered based on their activity in Becquerel for a given recorded decay time. The absolute yield of the primary gamma-ray energy for each fission product were considered when ordering the nuclides that should be represented in the delayed gamma spectra.

Table 4.3: Fission products with the highest activity for a sample that was recorded for 1 second after irradiation.

Radionuclide	Half-Life	Primary Gamma-Ray Energy (keV)	Absolute Yield	Present in beam chopper spectrum?
^{97}Sr	429 ms	1905	25	Yes
^{98}Y	0.548 s	1223	36	Yes
^{99}Zr	2.1 s	469.137	55.2	Yes
^{142}Cs	1.70 s	359.598	27.2	Yes
^{96}Sr	1.07 s	122.297	76.5	Yes
^{95}Rb	377.5 ms	204	15.092	Yes
^{101}Zr	2.3 s	205.7	6.1	Yes
^{98}Sr	0.653 s	119.353	73	No
^{99}Y	1.470 s	121.761	46.9	Yes

Table 4.4: Fission products with the highest activity for a sample that was recorded for 10 seconds after irradiation..

Radionuclide	Half-Life	Primary Gamma-Ray Energy (keV)	Absolute Yield
^{97}Y	3.75 s	3287.6	18.1
^{92}Rb	4.492 s	814.98	33
^{99}Zr	2.1 s	469.137	55.2
^{100}Nb	1.5 s	535.666	45.7
^{100}Zr	7.1 s	400.48	19.2
^{102}Nb	1.3 s	296	79.38
^{142}Cs	1.70 s	359.598	27.2
^{96}Sr	1.07 s	122.297	76.5
^{101}Zr	2.3 s	205.7	6.1

Table 4.5: Fission products with the highest activity for a sample that was recorded for 1 minute after irradiation.

Radionuclide	Half-Life	Primary Gamma-Ray Energy (keV)	Absolute Yield	Present in on/off spectrum?
^{94}Sr	75.3 s	1427.7	94.2	Yes
^{93}Sr	7.423 min	590.238	68	Yes
^{140}Cs	63.7 s	602.35	52.5	No
^{100}Nb	1.5 s	535.666	45.7	Yes
^{137}Xe	3.818 min	455.49	31.2	No
^{138}Xe	14.08 min	258.411	31.5	No
^{95}Y	10.3 min	954	15.8	Yes
^{98}Nb	2.86 s	787.4	13	No
^{139}Cs	9.27 min	1283.23	8.3	No

Table 4.6: Fission products with the highest activity for a sample that was recorded for 1 hour after irradiation.

Radionuclide	Half-Life	Primary Gamma-Ray Energy (keV)	Absolute Yield
^{94}Sr	75.3 s	1427.7	94.2
^{93}Sr	7.423 min	590.238	68
^{140}Cs	63.7 s	602.35	52.5
^{100}Nb	1.5 s	535.666	45.7
^{137}Xe	3.818 min	455.49	31.2
^{138}Xe	14.08 min	258.411	31.5
^{95}Y	10.3 min	954	15.8
^{98}Nb	2.86 s	787.4	13
^{139}Cs	9.27 min	1283.23	8.3

Table 4.7: Fission products with the highest activity for a sample that was recorded for 8 hours after irradiation.

Radionuclide	Half-Life	Primary Gamma-Ray Energy (keV)	Absolute Yield
^{134}I	52.5 min	847.025	95.4
^{138}Cs	33.41 min	463	98
^{93}Sr	7.423 min	590.238	68
^{94}Y	18.7 min	918.74	56
^{134}Te	41.8 min	767.2	29.5
^{137}Xe	3.818 min	455.49	31.2
^{138}Xe	14.08 min	258.411	31.5
^{95}Y	10.3 min	954	15.8
^{139}Cs	9.27 min	1283.23	8.3

The ORIGEN-ARP results were used to start the identification of the peaks in the uranium spectrum. Although some of the primary gamma-rays have energies that are in the x-ray range and therefore not recorded by the system, the ORIGEN-ARP data provided a starting point for the fission product identification.

4.5 DETECTION LIMITS

The minimum amount of ^{235}U necessary to locate the photopeak of a gamma-ray 95% of the time was calculated for the peaks attributed to a single fission product. Using

equation (2.15) with k=1.645 and the limiting mean of the blank is the continuum counts at the peak energy, the detection limit in counts is calculated. Assuming the activity of the sample due to a specific nuclide can be described by

$$A \approx \phi \frac{\sigma_f \cdot m \cdot N_a}{MW} \chi_i \tag{4.5}$$

where ϕ is the flux of the reactor, σ_f is the fission cross section of ^{235}U, m is the mass of ^{235}U in grams, N_a is Avogadro's Number, MW is the molecular weight of ^{235}U, and χ_i the fission yield of the specific fission product. Therefore, we can relate the detection limit to the equation as

$$L_D = A\gamma_i\varepsilon = \phi\frac{\sigma_f \cdot m \cdot N_a}{MW}\chi_i\gamma_i\varepsilon \tag{4.6}$$

By solving for the mass of ^{235}U, the minimum amount of ^{235}U to detect a given fission product is calculated.

$$m = \frac{L_D \cdot MW}{\sigma_f N_a \phi \chi_i \gamma_i \varepsilon} \tag{4.7}$$

For the calculations, the flux of the reaction in beamport three is 4×10^6 n·cm^{-2}·s^{-1} [33], but we had to consider that the beam chopper allows irradiation for only a quarter of the time.

Using equation (4.7), the minimum amount of ^{235}U necessary to detect a specific peak 95% of the time was calculated. The equation provides the amount in grams necessary to produce enough of the fission product to release enough gamma-rays of a specific energy. Table 4.8 shows the amount of ^{235}U need in grams to be able to detect the peak created by the gamma-ray emitted by the fission product in 95% of the spectra

collected. The detection limits in Table 4.8 are only applicable to the set-up at The University of Texas using the beam chopper method. The prompt method only account for 7 of the 27 peaks, and the mass of uranium necessary for the peaks to be present in the spectrum is on the order of 10 to 100 times the amounts summarized in Table 4.8.

Table 4.8: The peaks are correlated to the fission products with gamma-rays that produced them.

Energy (keV)	Nuclide	Uranium needed (g)	Error
277.61	^{96}Sr	12.89	0.760
440.99	^{101}Nb	19.39	9.720
555.73	^{141}Cs	30.69	2.663
724.7	^{99}Y	13.91	1.131
780.94	^{101}Zr	83.62	9.361
787.86	^{98}Nb	7.13	0.566
840.24	^{98m}Y	84.50	4.736
1147.77	^{141}Cs	67.82	7.816
1218.45	^{92}Kr	6.07	0.482
1293.62	^{97}Y	19.10	1.903
1537.72	^{90}Kr	12.45	1.902
1633.19	^{102}Nb	6.74	1.115
1750.77	^{96}Y	29.74	8.229
1904.35	^{97}Sr	5.09	1.989
2015.6	^{144}Cs	266.30	30.861
2175.61	^{144}Cs	277.05	100.340
2289.46	^{136}I	14.11	9.949
2415.64	^{136}I	22.78	12.035
2590.69	^{91}Kr	217.40	349.380
2631.28	^{134}Sb	5.58	1.207
2639.33	^{100}Y	8.11	0.959
2717.38	^{95}Sr	14.34	14.337
2942.49	^{98}Y	9.79	10.012
2960.46	^{136}I	165.49	168.833
3287.48	^{97}Y	3.95	1.958
3599.63	^{91}Rb	5.64	1.736
4019.91	^{93}Rb	165.88	167.320
4134.49	^{90}Rb	11.38	2.354

Chapter 5: Conclusions and Recommendations

The traditional prompt gamma activation analysis of a uranium sample provides only a few peaks to identify a sample as uranium. The majority of the peaks in the prompt uranium spectrum are attributed to fission products. However, counting the sample while the beam was blocked allowed the spectral peaks produced by the short-lived fission products to stand out in the spectrum. The detection limits of the peaks attributed to a single nuclide in the beam chopper spectrum were calculated to provide a comparison between gamma-rays at different energy levels.

The detection limits also allowed the examination of the technique as a practical security application. The current IAEA safeguards "significant quantities" of uranium, which is currently 25 kg of uranium that is over 20% enriched [37]. The NRDC recommends safeguards enriched uranium over 3 kg. There are 27 peaks attributed to a single fission product in the beam chopper spectrum that require significantly less than that amount to detect the peak 95% of the time. There peaks require less than 0.3 kg of ^{235}U, which is below the proposed "significant quantity" of enriched uranium set by the NRDC.

The MOX fuel pellet produced prompt and delayed spectra without any viable peaks. Further investigations of the shielding properties of the sample are necessary. One of the obvious next steps would be to examine the fission product spectra for a plutonium foil sample. The IAEA requirements states that a "significant quantity" of plutonium is over 8 kg [37]. Judging from the detection limits of the uranium sample, the detection of plutonium could be easily quantified with the fission product spectrum.

In the future, uranium samples with different enrichment levels could be examined. In order to quantify enrichment using only a delayed spectrum, the ratio between different fission products could be examined. ^{238}U is a fertile material that converts to ^{239}Pu. Through comparison of the ^{239}Pu fission yields, the ratios could be possibly be differentiated.

Other future work includes deconstructing individual peaks with multiple nuclide composition. This would be completed using fission product yields, gamma-ray yields, the area of the peak in question, and the area of the peaks attributed to single nuclides. This process would aid in the enrichment ratios by allowing a larger number of fission products to be quantified.

Appendix A

Fission products with corresponding peaks from the spectrum collected using the beam chopper.

Isotope	Half-Life	Energy Levels (keV)
^{74}Zn	95.6 s	142.55
^{75}Zn	10.2 s	431.54
^{76}Cu	0.641 s	431.54
^{77m}Ge	52.9 s	1677.91
^{78}Ga	5.09 s	566.57
^{79}Ga	2.847 s	142.55
^{80}Zn	0.545 s	175.83, 312.87, 462.99, 566.57, 613.52, 642.01, 686.46, 710.75, 735.76, 757.33, 1333.17, 1501.93
^{80}Ge	29.5 s	933.27, 1010.4, 1118.82, 1564.63
^{80}Ga	1.697 s	586.10, 658.61, 1010.40, 1313.31, 1677.91
^{81}Ga	1.217 s	529.84, 710.75, 2441.73
^{81}Ge	7.6 s	793.85
^{82}As	19.1 s	654.06, 1079.08, 1970.91
^{83}Ge	1.85 s	307.5, 1413.82, 1435.96, 1525.05, 2196.02, 3033.77
^{85}Se	31.7 s	345.34, 1428.01, 3400.90
^{86}Se	15.3 s	382.05
^{86}Br	55.0 s	1391.5, 2752.73
^{87}Br	55.60 s	2005.19
^{87}Se	5.29 s	242.94, 469.44, 710.75, 1304.51
^{88}Se	1.52 s	259.26, 408.37
^{88}Br	16.5 s	775.48, 799.39, 1577.40
^{89}Br	4.40 s	953.89, 1000.99, 1096.80
^{89}Rb	15.15 min	2196.02, 2570.18
^{90}Kr	32.2 s	120.52, 242.94, 541.0, 1118.82, 1537.72
^{90m}Rb	258 s	824.93, 832.03

^{90}**Rb**	158 s	832.03, 4134.49, 4642.49
^{91}**Rb**	58.4 s	345.34, 1970.91, 3599.63
^{91}**Kr**	8.57 s	398.03, 505.58, 613.52, 1501.93, 2590.69, 2752.73
^{92}**Kr**	1.840 s	142.55, 317.23, 546.76, 876.46, 1218.45
^{92}**Rb**	4.492 s	816.14, 1384.13, 2820.86, 4642.49
^{93}**Rb**	5.84 s	211.86, 219.33, 431.54, 710.75, 1384.13, 1806.68, 4019.91
^{94}**Kr**	0.20 s	136.25, 186.44, 191.6, 219.33, 317.23, 358.58, 595.57, 697.37, 767.89,
^{94}**Rb**	2.702 s	837.07, 1577.40
^{94}**Sr**	75.2 s	1428.01
^{95}**Rb**	377.5 ms	352.39, 578.43, 1260.58
^{95}**Sr**	23.90 s	686.46, 824.93, 943.72, 1278.85, 2717.38
^{95}**Y**	10.3 min	1806.68
^{96}**Sr**	1.06 s	120.52, 277.61, 529.84, 595.57, 809.51, 933.27
^{96}**Rb**	0.199 s	691.84, 816.14
^{96}**Y**	5.34 s	919.18, 1750.77
^{97}**Y**	3.75 s	296.99, 1103.33, 1293.62, 1400.14, 3287.48, 3400.90
^{97}**Sr**	426 ms	307.5, 654.06, 697.37, 799.39, 953.89, 1260.58, 1904.35
^{97}**Rb**	169.9 ms	417.60, 686.46
^{98m}**Y**	2.0 s	622.05, 647.72, 840.24, 1223.64
^{98}**Nb**	2.86 s	647.72, 787.86
^{98}**Rb**	114 ms	1835.81
^{98}**Y**	0.548 s	1223.64, 2942.49
^{98m}**Y**	2.0 s	751.08
^{99}**Sr**	270 ms	120.52, 535.99
^{99}**Y**	1.470 s	120.52, 535.99, 578.43, 602.87, 613.52, 724.7,
^{99}**Zr**	2.1 s	388.55, 462.99, 469.44, 546.76
^{100}**Y**	0.94 s	120.52, 211.86, 613.52, 864.62, 876.46, 1096.8, 2439.39, 2639.33
^{100}**Nb**	1.5 s	535.99, 622.05, 767.89, 970.06, 1501.93
^{100m}**Nb**	2.99 s	1278.85

^{100}**Zr**	7.1 s	499.97
^{101}**Sr**	118 ms	164.17, 462.99, 590.62, 1000.99
^{101}**Zr**	2.3 s	206.07, 780.94, 913.50
^{101}**Nb**	7.1 s	440.99
^{102}**Mo**	11.3 min	136.25, 149.26, 211.86, 358.58
^{102}**Sr**	69 ms	149.26, 255.65, 1103.33
^{102}**Nb**	1.3 s	296.99, 398.03, 402.54, 551.58, 654.06, 847.20, 948.67, 1633.19
^{102}**Y**	0.3 s	743.26
^{103}**Tc**	54.2 s	499.97
^{103}**Y**	0.23 s	107.35, 149.26, 259.26
^{103}**Zr**	1.3 s	120.52, 149.26, 164.17
^{103}**Nb**	1.5 s	138.73, 242.94, 455.24, 505.58, 642.01
^{104}**Tc**	18.3 min	1677.91
^{105}**Nb**	2.95 s	138.73, 149.26, 191.6, 232.41, 307.5
^{106}**Mo**	8.4 s	462.99, 505.58, 595.57
^{108}**Nb**	0.19 s	191.60, 585.10, 590.62
^{108}**Tc**	5.17 s	242.94, 1118.82
^{109}**Ru**	34.5 s	206.07, 358.58, 424.62, 888.63, 1010.40, 1304.51, 1501.93
^{110}**Tc**	0.92 s	242.94, 424.62, 1223.64, 1391.5, 1413.82, 1577.40, 1806.68
^{111}**Rh**	11 s	191.60
^{111}**Ru**	2.12 s	211.86, 307.50, 382.05, 847.2, 1268.39, 1400.14
^{112}**Rh**	2.1 s	388.55, 541.00
^{112}**Tc**	0.28 s	408.37
^{113}**Ru**	0.80 s	211.86
^{114}**Rh**	1.85 s	317.23
^{115}**Rh**	0.99 s	164.17
^{115m}**Ag**	18.0 s	388.55
^{116}**Rh**	0.68 s	398.03, 743.26
^{116}**In**	14.10 s	462.99

^{117}**Pd**	4.3 s	402.54
^{117m}**Ag**	5.34 s	686.46
^{120}**Ag**	1.23 s	505.58, 697.37, 816.14
^{120}**In**	3.08 s	2392.17
^{121}**Ag**	0.78 s	312.87, 352.39, 499.97, 816.14
^{121}**In**	23.1 s	919.18
^{122}**In**	1.5 s	948.67, 1391.5
^{123}**Ag**	0.309 s	743.26
^{123}**In**	5.98 s	535.99, 1131.8
^{124}**Cd**	1.25 s	142.55
^{124}**Ag**	0.172 s	462.99, 535.99, 613.52, 837.07, 1337.17
^{124}**In**	3.11 s	970.06, 1131.80
^{125}**Cd**	0.65 s	435.26
^{125}**In**	2.36 s	1032.29, 1333.17
^{126}**Cd**	0.506 s	686.46
^{128}**Cd**	0.34 s	462.99, 857.55
^{129}**In**	0.61 s	767.89, 1010.40, 1137.26
^{133}**In**	180 ms	857.55, 1564.63, 2005.19
^{134}**Sb**	0.78 s	1278.85, 2631.28
^{135}**Sb**	1.68 s	658.61, 1268.39, 1835.81, 2570.18
^{136m}**I**	46.9 s	913.5, 1313.31
^{136}**I**	83.4 s	1313.31, 2289.46, 2415.64, 2960.46
^{137}**Te**	2.49 s	242.94, 358.58, 469.44, 551.58, 602.87, 710.75, 895.30
^{138m}**Cs**	2.90 min	107.35, 1435.96
^{140}**I**	0.86 s	566.57
^{140}**Xe**	13.60 s	120.52, 211.86, 622.05, 654.06, 775.48, 809.51, 1137.26, 1313.31, 1413.82,
^{141}**Xe**	1.73 s	541.00
^{141}**Cs**	24.94 s	555.73, 586.1, 691.84, 1147.77
^{142}**Xe**	1.22 s	191.60

^{142}Cs	1.70 s	358.58, 1278.85
^{143}Cs	1.77 s	191.60, 219.33, 658.61
^{143}Ba	14.33 s	211.86, 431.54, 799.39, 895.30, 1010.40
^{144}Ba	11.5 s	388.55, 431.54, 541.00,
^{144}Cs	1.01 s	1079.08,1118.82, 2015.60, 2175.61
^{144}La	40.8 s	1525.05
^{145}La	24.8 s	164.17, 352.39, 358.58
^{145}Cs	0.594 s	175.83, 242.94, 435.26, 455.24, 546.76, 751.08
^{145}Ba	4.31 s	417.60
^{146}Cs	0.321 s	307.5, 735.76, 933.27, 1970.91
^{147}La	4.015 s	120.52, 186.44
^{152}Pr	3.63 s	164.17
^{153}Pr	4.28 s	191.60
^{153}Nd	31.6 s	255.65, 345.34, 417.60
^{154}Pr	2.3 s	164.17, 793.85, 895.3, 933.27,
^{155}Nd	8.9 s	888.63
^{157}Pm	10.56 s	164.17
^{160}Eu	38 s	175.83, 824.93, 1000.99, 1304.51, 1384.13

Appendix B

Fission products with corresponding peaks from the spectrum collected using the1 min on/off method.

Nuclide	Half-Life	Gamma-Ray Energies (keV)
^{100}Tc	15.8 s	540.97, 590.6, 1203.49
^{101}Mo	14.61 m	190.87, 192.75, 408.14, 498.76, 506.1, 590.6, 607.92, 641.89, 697.2, 871.36, 933.03, 1010.12, 1061.08, 1160.78, 1304.6, 1532.07, 1597.82, 2031.25, 2040.01
^{102}Nb	4.3 s	551.1, 846.89, 1634.09
^{102}Tc	5.28 s	475.56, 627.09, 631.37, 636.44, 864.13, 1102.73, 1196.96, 1239.97, 1613.95, 2246.74
^{103}Tc	54.2	136.67, 211.45, 344.41, 346.33, 388.80, 402.79, 562.07
^{104}Tc	18.3 m	358.12, 530.09, 535.83, 884.16, 895.18, 1597.82, 1613.95, 1676.84
^{106}Tc	36 s	270.01, 1970.49, 2237.62
^{109}Rh	80 s	291.23, 325.69, 424.62
^{109}Ru	34.5 s	205.94, 225.87, 358.12, 424.62, 1010.12, 1304.6, 1501.63, 1537.4, 1756.5, 1835.93
^{110}Rh	28.5 s	369.84, 440.23, 546.64, 839.66, 904.96
^{113}Pd	93 s	96.76, 270.01, 462.88, 482.96, 658.12
^{115}Pd	25 s	247.47, 304.59, 344.41, 397.81, 555.42
^{116}Pd	11.8 s	92.14
^{117}Ag	72.8 s	136.67, 157.31, 312.62, 468.25, 1996.42, 2014.88, 2246.74
^{117m}Ag	5.34 s	136.67, 157.31, 205.94, 219.43, 297.08, 307.37, 686.02
^{120}In	46.2 s	250.67, 636.44, 864.13
^{121}Cd	13.5 s	1041.14
^{121}In	23.1 s	259.11, 658.12, 918.88, 925.5
^{121m}In	3.88 m	908.55, 1041.14, 1102.73, 1118.44
^{128}Sb	10.4 m	192.75, 312.62, 743.17, 787.76, 1041.14, 1160.78
^{129m}Sn	6.9 m	219.43, 264.63, 307.37, 506.1, 602.78, 1131.19, 1160.78

^{129}Sn	2.23 m	578.31, 647.54, 1196.96
^{130m}Sb	6.3 m	182.35, 369.84, 468.25, 498.76, 647.54, 793.64, 816.88, 839.66, 1017.52
^{130}Sn	3.72 m	150.39, 190.87, 192.75, 435.05, 551.1, 743.17, 780.15
^{131}Sb	23.03 m	641.89, 658.12, 933.03, 943.44, 1123.80
^{132}Sb	2.79 m	102.52, 150.39, 277.82, 291.23, 381.87, 498.76, 636.44, 697.2, 816.88, 974.43
^{133}Sb	2.5 m	816.88, 1095.89, 1304.6, 1551.15, 1727.66, 2414.95
^{136}I	83.4 s	1312.92, 1322.1, 2289.45, 2414.95, 2866.6
^{136m}I	46.9	197.69, 346.33, 369.84, 381.87, 482.96, 913.26, 1312.92, 1740.44
^{137}Xe	3.818 m	394.07, 455.25, 1613.95, 2849.58
^{137}Xe	3.818 m	1613.95
^{138}Cs	33.41 m	546.64, 871.36, 1435.52, 2217.31
^{138m}Cs	2.90 m	190.87, 192.75, 462.88, 871.36, 1435.52
^{138}Xe	14.08 m	242.81, 259.11, 397.81, 435.05, 1768.1, 2004.88, 2014.88, 2252.39
^{139}Cs	9.27 m	627.09, 1283.03, 1420.16, 2349.58
^{140}Cs	63.7 s	602.78, 908.55, 1634.09, 1851.57, 2100.9, 2237.62, 2330.21, 2521.62
^{140}Xe	13.60 s	120.39, 555.42, 607.92, 621.86, 775.41, 805.62, 925.5, 989.88, 1137.38, 1312.92, 1413.86
^{141}Cs	24.94 s	555.42, 562.07, 586.06, 1147.43, 1196.96
^{142}Ba	10.6 m	232.13, 255.61, 312.62, 364.54, 424.62, 839.66, 895.18, 948.48, 1000.95, 1078.62, 1095.89, 1203.49
^{143}Ba	14.33 s	211.45, 255.61, 291.23, 431.31, 435.05, 719.65, 799.00, 895.18, 925.5, 980.07, 1010.12, 1196.96
^{143}La	14.14 m	455.25, 621.86, 641.89
^{144}La	40.8	397.81, 540.97, 586.06, 735.7, 846.89, 1524.66, 1970.49
^{145}Ba	4.31 s	92.14, 96.76, 163.94, 190.87, 381.87, 417.78, 492.26, 546.64
^{145}Ce	3.01 m	232.13, 285.5, 351.86, 424.62, 440.23, 724.46, 857.57, 1108.07, 1147.43
^{145}La	24.8 s	163.94
^{146}La	10.0 s	182.35, 259.11, 291.23, 408.14, 455.25, 667.2, 925.50

^{148}Ce	56 s	102.52, 120.39, 270.01, 291.23, 325.69, 351.86
^{148}Pr	2.27 m	302.22, 451.32, 613.15, 636.44, 658.12, 697.2, 719.65, 1248.24
^{149}Ce	5.3 s	87.35, 144.04, 381.87
149Pr	2.26 m	107.82, 139.23, 166.35, 259.11, 317.03, 333.93
^{151}Nd	12.44 m	87.35, 139.23, 169.1, 255.61, 424.62, 586.06, 677.3, 735.7, 739.11, 799.00, 1017.52, 1123.80
^{152m}Pm	7.52 m	242.81, 780.15, 1095.89, 1435.52
^{153}Nd	31.6 s	107.82, 285.5, 344.41, 417.78, 475.56, 969.43
^{154}Pm	1.73 m	546.64, 969.43, 1147.43
^{155}Nd	8.9 s	87.35, 182.35, 186.29, 219.43, 417.78, 607.92, 953.62
^{155}Pm	41.5 s	408.14, 724.46, 780.15
^{156}Pm	26.70 s	175.63, 933.03, 1147.43, 1260.33
^{157}Sm	482 s	197.69, 317.03, 394.07, 989.88, 1464.84
^{159}Eu	18.1 m	96.76, 144.04, 677.3, 805.62
^{160}Eu	38 s	175.63, 1383.75
^{68}Cu	31.1 s	578.31, 1078.62, 1260.33, 1676.84
^{74}Ga	8.12 m	492.26, 595.92, 607.92, 867.86, 1000.95, 1203.49, 1333.03, 1939.32
^{75}Ga	126 s	175.63, 250.67, 578.31, 884.16, 1248.24
^{76}Ga	32.6 s	562.07
^{78}Ga	5.09 s	566.43, 621.86
^{80}As	15.2 s	667.2, 1293.97
^{80}Ge	29.5 s	264.63, 933.03, 1118.44, 1260.33, 1564.39
^{81}As	33.3 s	388.8, 468.25, 492.26, 2100.9
^{81}Ge	7.6 s	92.14, 793.64, 876.16
^{83}As	13.4 s	735.7, 1333.03, 2077.84
^{83m}Se	70.1 s	989.88, 1031.92
^{83}Se	22.3 m	358.12, 719.65, 799.00, 888.61

^{84}Br	31.80 m	2483.67, 3927.61
^{85}Br	2.90 m	805.62, 864.13, 918.88, 1727.66
^{85}Se	31.7 s	344.41, 431.31, 607.92, 839.66, 943.44, 953.62, 1203.49, 1427.55
^{86}Br	55.0 s	1217.55, 1464.84, 1564.39, 2349.58, 2751.87
^{86}Se	15.3 s	381.87, 1118.44, 1277.79, 2237.62, 2441.68, 2662.02
^{87}Br	55.60 s	530.09, 831.79, 943.44, 1023.72, 1413.86, 1420.16, 1577.8, 1835.93, 2004.88, 2706.02, 2997.22, 4180.23
^{87}Se	5.29 s	242.81, 333.93, 468.25
^{88}Br	16.5 s	775.41, 805.62, 1577.8
^{88}Rb	17.78 m	1383.75, 1835.93
^{89}Kr	3.15 m	219.43, 498.76, 586.06, 739.11, 867.86, 904.96, 974.43, 1108.07, 1322.1, 1473.23, 1501.63, 1532.07, 1694.07, 1901.63, 1939.32, 2100.9, 2866.6, 3533.57
^{89}Rb	15.15 m	658.12, 948.48, 1031.92, 1248.24, 1537.40, 2195.38, 2569.43, 2706.02
^{90}Kr	32.32 s	120.39, 242.81, 540.97, 555.42, 1017.52, 1537.4
^{90m}Rb	258 s	831.79, 1061.08, 1375.98, 1664.89, 2127.47, 2751.87, 3316.31
^{90}Rb	158 s	831.79, 1061.08, 3303.51, 3382.57, 3533.57, 4134.45, 4364.94, 4645.76
^{91}Kr	8.57 s	107.82, 397.81, 506.1, 555.42, 613.15, 1023.72, 1102.73, 1108.07, 1137.38, 2483.67, 3112.55
^{91}Rb	58.4 s	92.14, 346.33, 440.23, 595.92, 602.78, 948.48, 1041.14, 1137.38, 1613.95, 1740.44, 1851.57, 1970.49, 2563.72, 2924.75, 3599.05, 4077.14
^{93}Sr	7.423 m	169.1, 259.11, 346.33, 590.6, 710.55, 876.16, 888.61, 1123.8, 1268.26, 1698.31
^{94}Sb	10.23 s	166.35, 297.08, 710.55, 1277.79
^{94}Sr	75.2	1427.55
^{95}Sr	23.90 s	686.02, 1277.79, 2246.74, 2716.05, 2932.67, 4077.14
^{95}Y	10.3 m	431.31, 953.62, 1322.1, 1806.48, 1939.32, 2174.96, 2631.82, 3575.06
^{96m}Y	9.6 s	144.04, 364.54, 913.26, 1108.07, 1225.39, 1750.34
^{99m}Nb	2.6 m	96.76, 351.86, 451.32, 535.83, 631.37, 2237.62, 2542.75, 2639.2, 2849.58

Appendix C

QUALITY ASSURANCE DATA SHEET
GEM SERIES HPGE (HIGH-PURITY GERMANIUM) COAXIAL DETECTOR SYSTEM

MODEL AND SERIAL NUMBERS

Detector Model No. GEM65P4
Cryostat Configuration PopTop
Dewar Model —
Preamplifier Model A257P
Preamplifier S/N 467
H.V. Filter Model 138EMI
H.V. Filter S/N 732
Smart-1 S/N —

IMPORTANT REFERENCE DATA

Ship Date 2-26-09
Serial No. 44-TP41444A

When calling Customer Service, always reference this Detector Serial No.

Dewar Capacity — Static Holding Time — Detector Cool-Down Time —

DIMENSIONS

Detector Diameter 74.4 mm
Detector Length 72.0 mm
End Cap to Detector 5 mm

ABSORBING LAYERS

Aluminum 1.00 mm
Magnesium — mm
Inactive Germanium 700 µm

RECOMMENDED OPERATING BIAS, POSITIVE 4500 V

PERFORMANCE SPECIFICATIONS*

	Warranted	Measured	Amplifier Time Constant
Resolution (FWHM) at 1.33 MeV, ^{60}Co	2.14 keV	1.79 keV	6 µs
Peak-to-Compton Ratio, ^{60}Co	66:1	88:1	6 µs
Relative Efficiency at 1.33 MeV, ^{60}Co	58.5 %	81.2 %	6 µs
Peak Shape (FWTM/FWHM), ^{60}Co	1.90	1.85	6 µs
Peak Shape (FWFM/FWHM), ^{60}Co		2.46	6 µs
Resolution (FWHM) at 122 keV, ^{57}Co	1100 eV	777 eV	6 µs

*Measured at a nominal rate of 1000 counts/s unless otherwise specified.

Other: Capsule NuCA #7284
Cryostat PH4 #7842

Data Certified by: BJ Wilson Date: 2-25-09

References

1. "Federal Fuding for Homeland Security: An Update," Economic and Budget Issue Brief. July 20, 2005.

2. "Q&A: North Korea nuclear talks" BBC World News website, http://news.bbc.co.uk/2/hi/asia-pacific/2340405.stm, accessed 2009.

3. F. Zakaria (Interviewer), F. Calderone (Interviewee), and G. Brown (Interviewee). Interview transcript. Retrived from CNN Web site: http://transcripts.cnn.com/TRANSCRIPTS/0902/01/fzgps.01.html

4. M. Calabresi, "Iran's Nuclear Threat," Time, March 8, 2003.

5. S. Pesente, G. Nebbia, M. Lunardon, G. Viesti, D. Sudac, K. Nad, S. Blagus, V. Valkovic, "Detection of hidden explosives by using tagged neutron beams with sub-nanosecond time resolution," Nucl. Instrum. Meth., A 53 (2004) 657-667.

6. N. K. Mumba, L. Vas, and Cs. M. Buczko, "Uranium and Thorium Analyses by Delayed Fission Neutron Counting Technique Using a Small Neutron Generator," J. Radioanal. Nucl. Chem., Letters 95, (1985) 311-322.

7. M. J. A. Armelin and M. B. A. Vasconcellos, "An Evaluation of the Delayed Neutron Counting Method for Simultaneous Analysis of Uranium and Thorium for $^{235}U/^{238}U$ Isotopic Ratio Determination," J. Radioanal. Nucl. Chem., 100 (1986) 37-47.

8. G. L. Molnar, Zs. Revay, T. Belgya, "Non-destructive interrogation of uranium using PGAA," Nucl. Instrum. Meth. in Phy. Res. B, 213 (2004) 389-393.

9. J. H. Moon, S. H. Kim, Y. S. Chung, J. M. Lim, G. H. Ahn, and M. S. Koh, "U determination in environmental samples by delayed neutron activation analysis in Korea," J. Radioanal. Nucl. Chem., 282 (2009) 33-35.

10. G. I. Kahlil and Cs. M. Buczko, "Simultaneous determination of U and Th by delayed fission neutron technique based on neutron generator," J. Radioanal. Nucl. Chem., 95 (1985) 101-110.

11. F. F. Dyer, J. F. Emery, K. J. Northcutt, R. M. Scott, "Determination of uranium and thorium in semiconductor memory materials by high fluence neutron activation analysis," J. Radioanal. Chem., 72 (1982) 53-67.

12. G. R. Keepin, T. F. Wimett, and R. K. Zeigler, "Delayed Neutrons from Fissionable Isotopes of Uranium, Plutonium, and Thorium," Phys. Rev., 107 (1957) 1044-1049.

13. X. Li, R. Henkelmann, and F. Baumgartner, "Rapid determination of uranium and plutonium content in mixtures through measurement of the intensity-time curve of delayed neutrons," Nucl. Instr. and Meth. in Phy. Res. B, 215 (2004) 246-251.

14. T. Gozani, "Nuclear Material Detection by Neutron Based Techniques," Rapiscan Systems Neutronics and Advanced Technologies Corporation (2006).

15. D. C. Glasgow, "Delayed neutron activation analysis for safeguards," J. Radioanal. Nucl. Chem., 276 (2008) 207-211.

16. E. Swanberg, E. B. Norman, H. Shugart, S. G. Prussin, and E. Browne, "Using low resolution gamma detectors to detect and differentiate ^{239}Pu and ^{235}U fissions," J. Radioanal. Nucl. Chem (2009) doi: 10.1007/s10967-009-0283-4

17. V. V. Verbinski, H. Weber, and R. E. Sund, "Prompt Gamma Rays from ^{235}U(n.f), ^{239}Pu(n,f), and Spontaneous Fission of ^{252}Cf," Phys. Rev. C, 7 (1973) 1173-1185.

18. R. W. Peelle and F. C. Maienschein, "Spectrum of Photons Emitted in Coincidence with Fission of 235U by Thermal Neutrons," Phys. Rev. C, 3 (1971) 373-390.

19. V. Polhorsky, J. Kliman, and J. Kristiak, "Prompt gamma-ray emission from fission of ^{239}Pu by resonance neutrons I," Czech. J. Phys., 43 (1993) 783-788.

20. B. Perot, C. Carasco, S. Bernard, A. Mariani, J. L. Szabo, G. Sannie, V. Valkovic, D. Sudac, G. Viesti, M. Lunardon, C. Botosso, G. Nebbia, S. Pesente, S. Moretto, A. Zenoni, A. Donzella, M. Moszynski, M. Gierlik, W. Klamra, P. Le Tourneur, M. Lhuissier, A. Colonna, C. Tintori, P. Peerani, V. Sequeira, and M. Salvato, "Measurement of 14 MeV neutron-induced prompt gamma-ray spectra from 15 elements found in cargo containers," App. Rad. and Iso., 66 (2008) 421-434.

21. D. Sudac, S. Blagus, and V. Valkovic, "Chemical composition identification using fast neutrons," App. Rad. and Iso., 61 (2004) 73-79.

22. R. Aryaeinejad, E. L. Reber, J. K. Jewell, J. D. Cole, and M. W. Drigert, "Fission process and its application in fissile material identification," J. Radioanal. Nucl. Chem., 264 (2005) 155-162.

23. Zs. Revay, T. Belgya, L. Szentmiklosi, and G. L. Molnar, "Prompt gamma activation analysis using a chopped neutron beam," J. Radioanal. Nuc. Chem., 264 (2005) 277-281.

24. D. Newman, Personal Webpage, accessed 2009, Retrieved from http://ffden-2.phys.uaf.edu/

25. Fission. (n.d.) In Wikipedia, accessed 2009, Retrieved from http://en.wikipedia.org/wiki/File:Fission_chain_reaction.svg#filehistory

26. "Uranium-235 Fission Yield vs. Mass Number," accessed 2009, Retrieved from http://www.tpub.com/content/doe/h1019v1/css/h1019v1_81.htm

27. Radioactive Decay. (n.d.) In Wikipedia, accessed 2009, Retrieved from [1] http://upload.wikimedia.org/wikipedia/commons/d/d8/Au198.PNG

28. G. L. Molnar (Ed.), "Handbook of Prompt Gamma Activation analysis with Neutron Beams," Springer, 2004.

29. R. J. Gehrke, J. R. Davidson, P. J. Taylor, R. G. Helmer, and J. W. Mandler, " Radioactinide additions to the electronic Gamma-ray Spectrum Catalogue," J. Radioanal. Chem., 248 (2001) 417-422.

30. G. R. Keepin, "Physics of Nuclear Kinetics," Addison-Wesley Publishing Company, Inc., Reading, Massachusetts, 1965.

31. L. A. Currie, "Limits of qualitative detection and quantitative determination. Application to radiochemistry," Anal. Chem, 40 (1968) 586-593.

32. Zs. Revay, R. K. Harrison, E. Alvarez, S. R. Biegalski, S. Landsberger, "Construction and characterization of the redesigned PGAA facility at The University of Texas at Austin," Nuc. Instr. and Meth. in Phys. Res. A, 577 (2007) 611-618.

33. E. Alvarez, "Characterization of the University of Texas Nuclear Engineering Teaching Laboratory Beam Port 3 Texas Cold Neutron Source-Prompt Gamma-

Ray Activation Analysis Facility," M.S.E. Thesis, The University of Texas at Austin (2005).

34. A. Brand, S. Biegalski, and L. Welch, "Development of a Neutron Beam Chopper at the University of Texas at Austin," ANS Transactions, Vol. 101 (2009) 344.

35. L. Szentmiklosi, Zs. Revay, and T. Belgya, "An improved beam chopper setup at the Budapest PGAA facility". Nuclear Instruments and Methods in Physics Research B 263 (2007) 90–94.

36. S.M. Bowman, L.C. Leal, "ORIGEN-ARP: Automatic Rapid Process for Spent Fuel Depletion, Decay, and Source Term Analysis," Vol. I, Sect. D (2000).

37. T. B. Cochran and C. E. Paine, "The Amount of Plutonium and Highly-Enriched Uranium Needed for Pure Fission Nuclear Weapons," Natural Resources Defense Council, Inc. NRDC (1995).

Vita

Christine Egnatuk was born in Albion, Michigan to Mary Ann and David Egnatuk. Egnatuk attended Albion Senior High School in Albion, Michigan. After graduating from high school in 1999, Egnatuk attended The College of Wooster in Wooster, Ohio where she was a mathematics and physics major. Egnatuk graduated in 2003. She worked in a neuroimaging research group under Dr. Jon-Kar Zubieta at The University of Michigan. Egnatuk is currently attending graduate school at The University of Texas at Austin in the Mechanical Engineering Department.

Email address: cegnatuk@gmail.com

This thesis was typed by the author.